REDOX REPORT
2025, VOL. 30, NO. 1, 2507557
https://doi.org/10.1080/13510002.2025.2507557

Taylor & Francis
Taylor & Francis Group

Varespladib attenuates *Naja atra*-induced acute liver injury via reversing Nrf2 signaling-mediated ferroptosis and mitochondrial dysfunction

Jiahao Liu[a], Linfeng Wang[a], Mengxia Xie[a], Wenjie Zhao[a], Jiaqi Sun[b], Yuji Jin[c], Meiling Liu[a], Jianqi Zhao[a], Lixia Cheng[a], Cheng Wen[d], Xiaowen Bi[a] and Chunhong Huang[a]

[a]School of Basic Medicine Sciences, Jiangxi Medical College, Nanchang University, Nanchang, People's Republic of China; [b]Queen Mary School, Jiangxi Medical College, Nanchang University, Nanchang, People's Republic of China; [c]Department of Basic Medicine, Jilin Medical University, Jilin, People's Republic of China; [d]School of clinical medicine, Jilin Medical University, Jilin, People's Republic of China

ABSTRACT

Objective: To investigate the protective effects of varespladib against *Naja atra*-induced acute liver injury (ALI) and to elucidate the toxic mechanism of snake venom phospholipase A_2 ($SVPLA_2$)-induced hepatic oxidative stress, with a particular focus on the role of Nrf2 signaling and its downstream pathways.

Methods: A combination of in vivo and in vitro models of *N. atra* envenomation was employed to assess liver injury, oxidative stress, and mitochondrial dysfunction. The interaction between $SVPLA_2$ and Nrf2 was analyzed, and the effects of varespladib treatment on these processes were evaluated using histological analysis, biochemical assays, and molecular techniques targeting oxidative stress, ferroptosis, mitophagy, and apoptosis.

Results: Varespladib significantly alleviated *N. atra*-induced ALI. $SVPLA_2$ was found to directly bind to Nrf2, leading to severe oxidative stress. This oxidative stress initiated a cascade involving Nrf2-mediated ferroptosis, mitochondrial dysfunction, excessive mitophagy, and mitochondria-dependent apoptosis. Treatment with varespladib effectively reversed these pathological events by inhibiting $SVPLA_2$ activity.

Conclusion: Varespladib shows strong therapeutic potential for *N. atra* envenomation by targeting $SVPLA_2$. Nrf2 was identified as a direct toxic target of $SVPLA_2$, and Nrf2-mediated ferroptosis and mitochondrial dysfunction were key mechanisms underlying $SVPLA_2$-induced hepatic injury.

KEYWORDS

Naja atra; snake venom; varespladib; Nrf2; ferroptosis; mitochondrial dysfunction; mitophagy; apoptosis

1. Introduction

Annually, approximately 5.4 million snakebites occur worldwide, directly leading to 1,800,000–2,700,000 envenomations and 80,000–140,000 fatalities [1,2]. In 2009, the World Health Organization (WHO) listed snakebite as a 'neglected tropical disease' (NTD) and further recognized it as the priority NTD in 2017 [3,4]. Snakebite poses a serious global threat, so it is necessary to enhance research on the toxic mechanisms and drug therapy.

In southern China, *Naja atra* (*N. atra*, Elapidae) is one of the most widely distributed venomous snakes [5]. Its venom comprises over 90% proteins and peptides, predominantly including snake venom phospholipase A_2 ($SVPLA_2$) (46.5%), three-finger toxins (3-FTxs) (42.8%), snake venom metalloproteinases (SVMPs) (1.5%), and other minor components [6,7]. Of these toxic elements, $SVPLA_2$ is the most abundant. Under physiological conditions, phospholipase A_2 (PLA_2) exists in multiple isoforms, including secretory PLA_2 ($sPLA_2$), calcium-independent PLA_2 ($iPLA_2$), and cytosolic PLA_2 ($cPLA_2$) [8]. These isoforms are critical in regulating various physiological and pathological processes [9]. Snake venom PLA_2 is categorized as $sPLA_2$, which specifically catalyzes the hydrolysis of ester bonds in glycerophospholipids at the sn-2 position, releasing free fatty acids and lysophospholipids [10,11]. Arachidonic acid (AA), one of the major free fatty acids released above, serves as a precursor to eicosanoids. These eicosanoids, including prostaglandins, thromboxane A_2, and leukotrienes, are key mediators of oxidative stress and inflammatory responses, leading to cytotoxicity [12], myotoxicity [13] and neurotoxicity [14]. Hence, $SVPLA_2$ is chiefly responsible for the toxicity of *N. atra* venom.

Clinically, *N. atra* envenomation commonly triggers serious visceral damage, such as acute liver injury (ALI) [15], acute heart failure [16], acute kidney injury (AKI) [17], and even multiple organ dysfunction syndrome [18]. ALI is the most common and severe complication [19]. Patients envenomed by *N. atra* venom exhibit elevated levels of liver biochemical indexes, oxidative stress indicators, and inflammatory indicators, including C-reactive protein (CRP), aspartate aminotransferase (AST), alanine aminotransferase (ALT), and lactate dehydrogenase (LDH) [20,21]. Moreover, Pałgan et al. demonstrated that even post-treatment, envenomed mice remain susceptible to hepatic injury, suggesting that the liver damage caused by snake venom is persistent rather than transient [21]. These results underscore the liver's heightened vulnerability to venom. However, the underlying mechanism is unclear.

Recent studies have recognized oxidative stress as a significant factor in venin-caused cellular damage [22–25]. $SVPLA_2$ exacerbates oxidative stress by disrupting cellular redox homeostasis, generating reactive oxygen species (ROS), decreasing antioxidant capacity, and causing mitochondrial dysfunction,

CONTACT Chunhong Huang chhuang@ncu.edu.cn School of Basic Medicine Sciences, Jiangxi Medical College, Nanchang University, Nanchang, Jiangxi 330006, People's Republic of China

which ultimately triggers apoptosis or necrosis [19,22]. Furthermore, studies also demonstrated that varespladib, a PLA_2 inhibitor, significantly protects hepatic cells from *N. atra* venom by reducing ROS production and mitigating mitochondrial dysfunction [19]. These findings all suggest that targeting oxidative stress and enhancing antioxidant defenses could be a promising therapy pathway for *N. atra*-triggered ALI. However, the toxic target and signaling pathway through which $SVPLA_2$ induces oxidative stress in hepatocytes remain to be investigated.

Nuclear factor erythroid 2-related factor 2 (Nrf2) is an important transcription factor that regulates cellular defense against oxidative stress, and its downstream targets include NADH dehydrogenase quinone 1 (NQO1) and heme oxygenase 1 (HO-1) [26–28]. Numerous studies emphasize the critical role of Nrf2 in safeguarding cells from animal toxin-induced damage [29–31]. However, its involvement in the toxic process of ALI induced by *N. atra* venom remains unclear. In addition to modulating cellular oxidative stresses, Nrf2 is also the key regulator of lipid peroxidation [32–34]. Our preliminary experiment revealed abnormally elevated iron ion content in the liver tissue of *N. atra*-envenomed mice, which decreased following varespladib treatment, indicating that the mechanism of $SVPLA_2$-induced ALI may involve the activation of the ferroptosis signaling pathway. Moreover, mitochondrial dysfunction is also regarded as a significant downstream mechanism of $SVPLA_2$-induced hepatocyte injury [16,19,35,36]. Besides ATP generation, mitochondria are essential for maintaining cellular redox homeostasis [37]. ROS frequently arise from electron leakage in the mitochondrial respiratory chain, impairing mitochondrial membrane potential (MMP), and ultimately triggering mitophagy [19]. Zhao et al. reported mitochondrial dysfunction and excessive mitophagy occurred in mice following exposure to *N. atra* venom, both mitigated by varespladib via inhibition of $SVPLA_2$, though the upstream regulatory mechanism has not been reported [19].

Developing and screening secure, efficient, and convenient antivenom drugs is urgently needed for treating and managing snakebite envenomations [38,39]. Recent findings emphasize that several Phase-2 approved drugs hold therapeutic promise, with varespladib, a PLA_2 inhibitor, emerging as one of the most notable candidates [40]. It has been extensively explored for treating snakebite envenomations [41]. Investigating the toxic target and mechanism is crucial for developing effective treatments and exploring potential applications [42]. Accumulating evidence suggests that $SVPLA_2$ induces serious hepatic oxidative stress [22], yet the potential mechanism needs to be further investigated. Taken together, this study explored the protective effects of varespladib on *N. atra*-induced ALI and the toxic mechanism of $SVPLA_2$-induced hepatic oxidative stress, focusing on Nrf2 signaling and its downstream pathways. This study shows that Nrf2 was identified as the direct toxic target of $SVPLA_2$, and Nrf2-mediated ferroptosis and mitochondrial dysfunction were the critical events in the toxic mechanism of $SVPLA_2$. Varespladib shows significant therapeutic potential for treating snakebite envenomation since its targeted inhibition of $SVPLA_2$.

2. Materials and methods

2.1. Main reagents

Varespladib was obtained from Shanghai Yuanye Biological Co., Ltd. (Shanghai, China). Lyophilized *N. atra* powders were supplied by the Huangshan Snake Hacienda (Huangshan, China). Dimethyl sulfoxide (DMSO), TRIzol reagent, reverse transcription kit were purchased from Gibco (Gaithersburg, U.S.A.). Antibodies against TNF-α and IL-6 were obtained from Wanlei Biotechnology Co., Ltd. (Shenyang, China). Primary antibodies targeting β-actin, Nrf2 (for WB), Nrf2 (for Co-IP), $sPLA_2$, HO-1, NQO-1, GPX4, ACSL4, Parkin, PTEN-induced kinase 1 (PINK1), Bcl-2, Bax, Cytochrome C (Cyt c), Cleaved Caspase-3, Cleaved Caspase-9, LC3-I and LC3-II, and HRP-conjugated goat anti-rabbit secondary antibodies were obtained from CST (Danvers, U.S.A.). MitoSOX™ Red Mitochondrial Superoxide Indicator was obtained from Invitrogen (California, U.S.A.). Lipofectamine® 8000 (Art.No. C0533), CCK-8 Kit, Cell Mitochondria Isolation kit, Assay kits for ATP production, mitochondrial membrane potential (MMP), ROS, and apoptosis were obtained from Beyotime Co., Ltd. (Shanghai, China). The colorimetric citrate synthase (CS) activity kit was acquired from Boxson Technology Co., Ltd. (Beijing, China). ALT, AST, iron ion content, total antioxidant capacity (TAC), total superoxide dismutase (SOD)-like, glutathione (GSH), total peroxidase, 8-hydroxy-2′-deoxyguanosine (8-OHdG), protein carbonyl (PC), Glutathione-dependent peroxidase, and malondialdehyde (MDA) assay kits were purchased from Jiancheng Biological Engineering Institute (Nanjing, China).

2.2. Animal ethics statement

6–8 week old male Kunming (KM) mice with a body weight approximately 30 ± 5 g, were obtained from the Animal Experiment Center of Nanchang University. All animal experiments were in accordance with the Experiment Guide of Nanchang University and were approved by the Ethics Committee (ethical code: NCULAE-20220624042).

2.3. Animal model and in vivo experimental design

Male KM mice were randomly divided into six groups ($n = 5$): (a) normal saline (NS), (b) DMSO only (DMSO), (c) DMSO with high-dose varespladib (DMSO + Var), (d) *N. atra* venom only (NA), (e) *N. atra* venom with low-dose varespladib (NA + Var-L), and (f) *N. atra* venom with high-dose varespladib (NA + Var-H) (Figure 1). In the NA group, *N. atra* venom was administered intraperitoneally at 0.5 times the lethal dose 50 (LD_{50}), corresponding to 27.5 mg/kg. Varespladib was dissolved in DMSO at 5 mg/mL and further diluted in vehicle solution to a final concentration of 2 mg/mL for follow-up experiments. For the drug-treated groups, low-dose varespladib was 30 μg and high-dose varespladib was 60 μg. These doses were determined based on previous experiments [19,40,43]. For all groups, the compounds were prepared in NS (150-μL volume), and incubated at 37°C for 15 min before intraperitoneal injection. After 12 h of injection, the mice were euthanized by CO_2 inhalation. Liver tissues were harvested for further analysis. Blood was collected via retro-orbitally using EDTA-coated syringes.

2.4. Cell culture and in vitro experiment design

The L02 cell line was purchased from Prosai Biological Co., Ltd. (Wuhan, China) and cultured in DMEM supplemented with 10% (v/v) FBS. Cells were maintained in a 5% CO_2 incubator at 37°C. The working doses of *N. atra* venom and

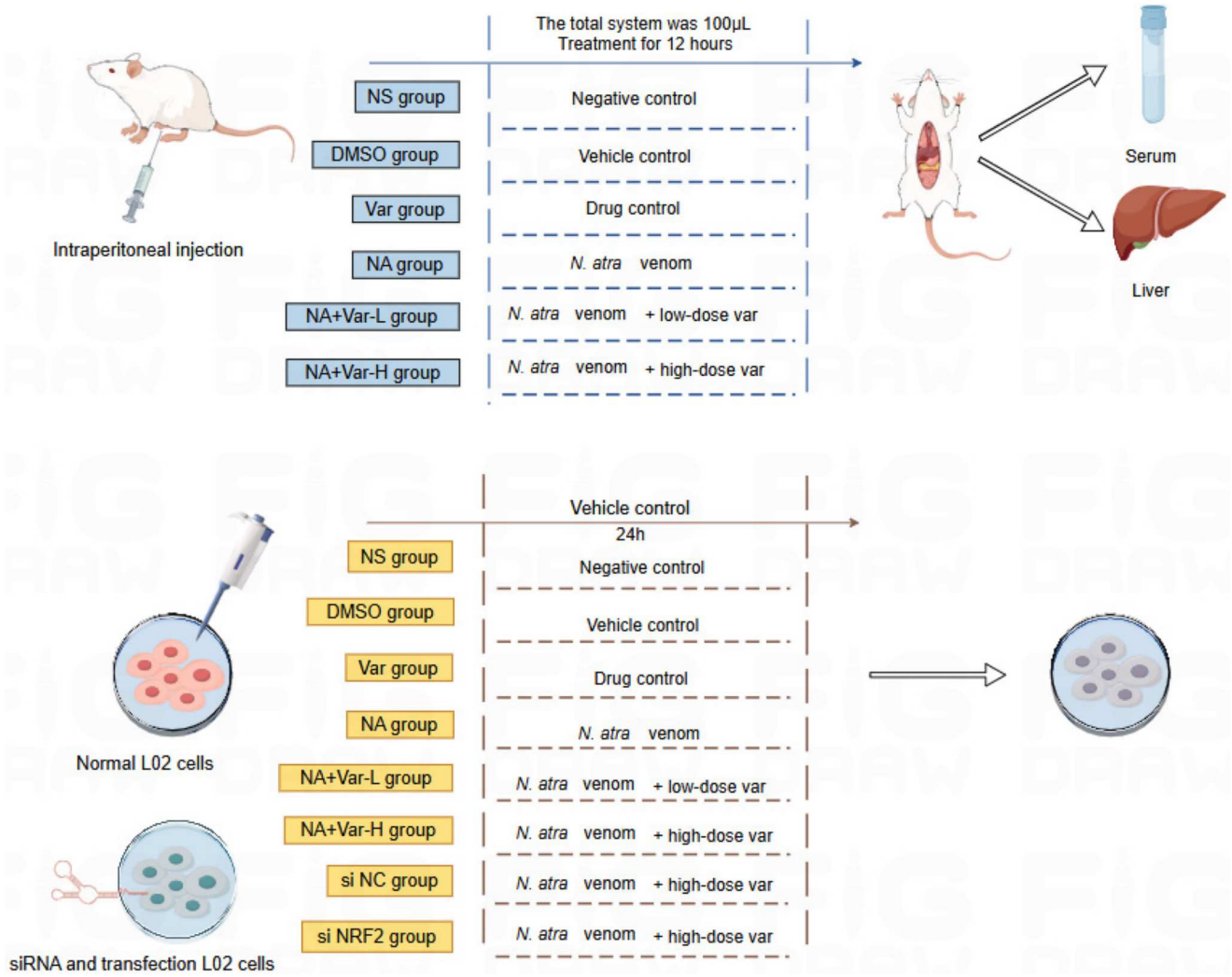

Figure 1. Schematic diagram of experimental design. (By Figdraw).

Varespladib were determined based on subsequent CCK-8 assays. Additionally, in vitro experiments included siRNA-transfected L02 cells, specifically the si NC (negative control) and si Nrf2 (Nrf2 knockdown) groups, which were treated with the same *N. atra* venom and high-dose drug concentrations. All groups were treated for 24 h Figure 1).

2.5. Cell viability assay

To assess the impacts of *N. atra* venom on L02 cell activity, a gradient dilution series was prepared with concentrations ranging from 20 μg/mL to 200 μg/mL in 20 μg/mL increments. Cell viability was detected by CCK-8 assay, following the manufacturer's instructions. GraphPad Prism 9.0 (GraphPad Software, U.S.A.) was used to calculate the half maximal inhibitory concentration (IC_{50}). To determine the inhibitory activity of varespladib against *N. atra* venom, the cells were incubated with *N. atra* venom at the IC_{50} dose. Increasing gradient of varespladib from 20 μg/mL to 200 μg/mL with an interval of 20 μg/mL was prepared and applied to the cells. The cell viability was measured as mentioned above.

2.6. siRNA and transfection

siRNA targeting Nrf2 and negative control siRNA were obtained from Santa Cruz Biotechnology (Santa Cruz, U.S.A.). The sequences of Nrf2 siRNA and negative control (NC) are shown in Table 1. L02 cells were transfected with the siRNA using Lipofectamine® 8000 reagent to knock down the Nrf2. Transfection was carried out when cells were 50%–60% confluent. Subsequent experiments were performed 24 h post-transfection.

2.7. Histological analysis

Hematoxylin and eosin (H&E) or periodic acid-Schiff (PAS) staining was conducted following established protocols [44–46].

Immunohistochemistry (IHC) analysis was conducted following standard procedures [44–46]. After standard treatment, the sections were incubated overnight with TNF-α (1:125, v/v) and IL-6 (1:125, v/v) primary antibodies at 4°C and incubated with a horseradish peroxidase – conjugated secondary antibody (1:200, v/v) for 1 h at room temperature. Diaminobenzidine staining was applied to visualize antigen expression. The Mean Optical Density of the IHC images was quantified using ImageJ software.

2.8. Sero-enzyme assay

Blood samples (1 ml) were collected from mice and centrifuged at 4000 RPM for 20 min. Serum levels of ALT and AST were measured using assay kits according to the manufacturer's protocols.

Table 1. The sequences of Nrf2 siRNA and negative control (NC).

siRNA name	Target gene	Sense strand (5′−3′)	Antisense strand (5′−3′)
si NRF2	Nrf2l2	CCACCAUCAUAGACGUUAdTdT	UAACGUCCUAUGAUGGUGGdTdT
si NC	Negative	UUCUCCGAACGUGUCACGUdTdT	ACGUGACACGUUCGGAGAAdTdT

2.9. Measurement of WBC counts

A 1 ml sample of mouse whole blood was collected with heparin anticoagulant. WBC counts were determined using a fully automated hematology analyzer (Jinan Hanfang Medical Equipment Co. Ltd., China).

2.10. Oxidative stress assays

Assays for oxidative stress markers were conducted using kits according to the instructions. The following parameters were assessed: TAC, Total peroxidase, Total SOD-like, GSH, Glutathione-dependent peroxidase, 8-OHdG, PC, MDA, and iron ion content.

2.11. Molecular docking

The structure of $sPLA_2$ (ID: 5Y5E) and Nrf2 (ID: 1X2R) were downloaded from the Protein Data Bank (https://www.rcsb.org/). Molecular docking was performed three times using GRAMM-X Docking Web (https://gramm.compbio.ku.edu/) [47]. Next, the best binding pose was visualized using PyMOL (v2.3.0). The evaluation of the binding degree was based on established criteria [48].

2.12. Molecular dynamics simulations (MDS)

MDS was carried out using the GROMACS 2019.6 software and conducted following established protocols [49]. The root mean square fluctuation (RMSF), root mean square deviation (RMSD), free energy map (FEL), and radius of gyrate (Rg) were calculated to evaluate the stability of the complexes.

2.13. Detection of ROS concentrations

ROS of the cells were assessed by fluorescence microscope (Nikon, Japan). Briefly, L02 cells after treatment were incubated with the fluorescent dye 2,7-dichlorofluorescein diacetate at 37°C for 40 min. After washing, the results were analyzed by fluorescence microscope.

2.14. Mitochondrial separation

Cell Mitochondria were separated using the Cell Mitochondria Isolation kit, following the manufacturer's protocols. This kit can obtain cytoplasmic proteins (free of mitochondria), and can be used to study the release of Cyt c into the cytoplasm.

Table 2. Primers used for real-time qRT-PCR.

Gene	Primer
Nfe2l2	F: GCTGCTCGGACTAGCCATT
	R: ATCAAATCCATGTCCTGCTGGG
Hmox1	F: TCAAGGCCTCAGACAAATCC
	R: ACAACCAGTGAGTGGAGCCT
Nqo1	F: CCGCATTCGTCTCTTGTCCG
	R: CGAAGTAACACAATGGGCTTGG
Gapdh	F: GCAAATTCAACGGCACAGTCAAG
	R: TCGCTCCTGGAAGATGGTGATG

2.15. Detection of mitochondrial functions

ATP production was measured following the manufacturer's protocols. CS activity was evaluated using a colorimetric assay kit. Mitochondrial ROS were detected as previously described. Cells with a density at 70%−80% were plated in a 12-well plate (black with a clear bottom) and incubated for 48 h. The cells were next exposed to 5 μM MitoSOX Red Mitochondrial Superoxide Indicator for 30 min at 37°C. Fluorescence was measured by a fluorescence microplate reader.

2.16. Detection of MMP

L02 cells after treatment were incubated with tetramethylrhodamine ethyl ester (TMRE) at 37°C for 35 min. Next, 4′,6-diamidino-2-phenylindole staining was applied. Fluorescence images were captured using a fluorescence microscope.

2.17. Apoptosis assay

Cell apoptosis was assessed by flow cytometry. Apoptosis was detected using the Annexin V-APC/PI Apoptosis kit, following the manufacturer's protocols.

2.18. Quantitative real-time PCR

Total RNA was isolated by conventional methods using TRIzol reagent and cDNA synthesis was carried out using a reverse transcription kit following the manufacturer's instructions. Quantitative real-time PCR was performed using SYBR Green dye on a Bio-Rad CFX Connect Real-Time PCR System (Bio-Rad). Data were analyzed using the $2^{-\Delta\Delta Ct}$ method, with *Gapdh* gene serves as the internal reference for normalization. Primer sequences used for qRT-PCR are detailed in Table 2.

2.19. Western blot analysis and Co-immunoprecipitation

Liver tissues and L02 cells were lysed with RIPA buffer. Denatured protein samples were separated by sodium dodecyl sulfate-polyacrylamide gel electrophoresis (SDS-PAGE) and transferred to polyvinylidene fluoride (PVDF) membranes. Following this, the membranes were blocked with blocking buffer (5% bovine serum albumin in Tris-buffered saline with Tween 20) for 2 h and incubated overnight with primary antibodies at 4°C. Primary antibodies targeting β-actin, Nrf2, HO-1, NQO-1, GPX4, ACSL4, Parkin, PINK1, Bcl-2, Bax, Cyt c, Cleaved Caspase-3, Cleaved Caspase-9, LC3-I and LC3-II were diluted in antibody diluent. Following three washes with Tris-buffered saline with Tween 20, the membranes were incubated with secondary antibodies (HRP-conjugated goat anti-rabbit) diluted at 1:5000 (v/v) for 1 h. Blots were visualized by the ECL

immunoblot detection system and band intensities were analyzed using Image J software.

For Co-IP, lysates of 1×10^7 L02 cells were immunoprecipitated with IP buffer containing IP antibody-coupled agarose beads, and protein–protein complexes were later subjected to Western blot. IgG was used as a negative control. The dilution ratios of all antibodies are as detailed in Table 3.

2.20. Statistical analysis

Statistical analyses and graphing were performed using GraphPad Prism 9.0. The normality of data distribution was assessed using the Shapiro – Wilk test. Data following a normal distribution were expressed as the mean ± SD and analyzed using parametric tests, including two-tailed unpaired Student's t-test for comparisons between two groups or one-way ANOVA for multiple group comparisons. For data not normally distributed, non-parametric tests were used. Differences were considered statistically significant at $p < 0.05$.

3. Results

3.1. Varespladib effectively mitigates N. atra-induced ALI

The histopathological changes in liver tissue were assessed by H&E and PAS staining. H&E staining revealed that the NA group exhibited extensive hepatocyte necrosis, blood-filled sinusoids, heavy inflammatory cell infiltration, narrowed or obliterated hepatic sinusoids, and loss of clear liver lobular structure. Varespladib treatment alleviated these pathological changes, with the Var-H group displaying only minor liver damage (Figure 2A). PAS staining demonstrated abnormal liver glycogen depletion in the NA group, which was reversed by varespladib treatment (Figure 2B). In addition, AST, ALT and the AST/ALT ratio were also increased after *N. atra* treatment. Varespladib treatment effectively reduced the levels of the above liver injury markers (Figure 2C–E). These results suggest that *N. atra* venom can induce ALI and varespladib can mitigate it in a dose-dependent manner.

3.2. Varespladib significantly alleviates N. atra-induced liver inflammation

N. atra venom commonly causes severe inflammation [19,50], and IHC was employed to evaluate the impact of varespladib on *N. atra*-induced liver inflammation. The results revealed significantly elevated expressions of TNF-α and IL-6 in venom-treated liver tissues, predominantly localized around the central veins. However, the inflammatory responses were markedly relieved following varespladib treatment (Figure 3A–D). Additionally, WBC counts, which were notably increased after *N. atra* venom exposure, were dose-dependently reduced by varespladib (Figure 3E). These results indicate that $SVPLA_2$ plays a pivotal role in *N. atra*-induced liver inflammation and that varespladib effectively alleviates this inflammation by inhibiting $SVPLA_2$.

Table 3. The dilutions of primary antibody used for WB and Co-IP.

Antibody	Dilution (v/v)	Antibody	Dilution (v/v)
β-actin	1:5000	Bcl-2	1:1000
Nrf2 (for WB)	1:2000	Bax	1:1000
HO-1	1:2000	Cyt c	1:2000
NQO-1	1:1000	Cleaved Caspase-3	1:1000
GPX4	1:1000	Cleaved Caspase-9	1:1000
ACSL4	1:2000	LC3-I	1:2000
Parkin	1:2000	LC3-II	1:2000
PINK1	1:1000	Nrf2 (for Co-IP)	1:1000
$sPLA_2$ (for Co-IP)	1:2000		

3.3. Varespladib protects the liver from N. atra-induced severe oxidative stress

Snake venom is known to induce severe oxidative stress [29,30]. To explore the hepatotoxic effects of *N. atra* on redox homeostasis and the protective role of varespladib, we analyzed typical oxidative stress markers. Compared to the NS group, the levels of TAC, total peroxidase, total SOD-like, GSH, and glutathione-dependent peroxidase were significantly reduced after *N. atra* venom exposure (Figure 4A–E). Moreover, oxidative damage to biomacromolecules were assessed using markers such as 8-OHdG, MDA, and PC, indicating damage to DNA, lipids, and proteins, respectively. The findings revealed that *N. atra*-induced lipid peroxidation was more pronounced than DNA and protein damage (Figure 4F–H). Importantly, varespladib mitigated these alterations in a dose-dependent manner. In summary, *N. atra* venom triggers significant hepatic oxidative stress, particularly lipid peroxidation, while varespladib effectively attenuates these effects by inhibiting PLA_2.

3.4. $SVPLA_2$ directly binds to Nrf2 to induce severe oxidative stress

Growing evidence suggests that oxidative stress is involved in the pathophysiology of snake toxins [29,30]. In this study, we also observed significant hepatic oxidative stress in mice injected with *N. atra* venom. Since Nrf2 is a significant transcription factor that regulates cellular defense against oxidative damage, we further explored its role in this pathological process. *In silico* analysis by molecular docking was conducted to explore the interactions between Nrf2 and $SVPLA_2$. Interestingly, a strong binding affinity was obtained (interface area = 2950.6 $Å^2$, $\Delta^iG = -34.8$ kcal/mol), with $SVPLA_2$ forming stable polar contacts with Nrf2, such as Gln-113 ($SVPLA_2$) combining with Lys-530 (Nrf2), Gly-135 ($SVPLA_2$) combining with Gln-61 (Nrf2) (Figure 5A).

Next, to assess the stability of the above binding, a 100-ns MDS was conducted. RMSD was the most important factor in describing the stability [51]. The lower the RMSD value, the better the binding stability. In this study, the RMSD values rose rapidly in the first 10 ns, followed by stabilization, with final average values ranging between 0.15 and 0.28 nm, which indicated that $SVPLA_2$ can tightly bind to Nrf2 during the simulation (Figure 5B). Additionally, the RMSF values were related to the interactions between $SVPLA_2$ and Nrf2. Commonly, low RMSF indicates a stable system and minimal residual motion. Most fluctuations of key residues involved in $SVPLA_2$-Nrf2 interaction were below 0.5 nm, further indicating system stability (Figure 5C). The Rg values were used to assess the overall shape and compactness of molecules, and lower Rg values commonly indicate a more compact molecule. In this study, the Rg values fluctuated between 3.4 and 3.8 nm, reflecting a stable, compact structure throughout the simulation (Figure 5D). FEL analysis

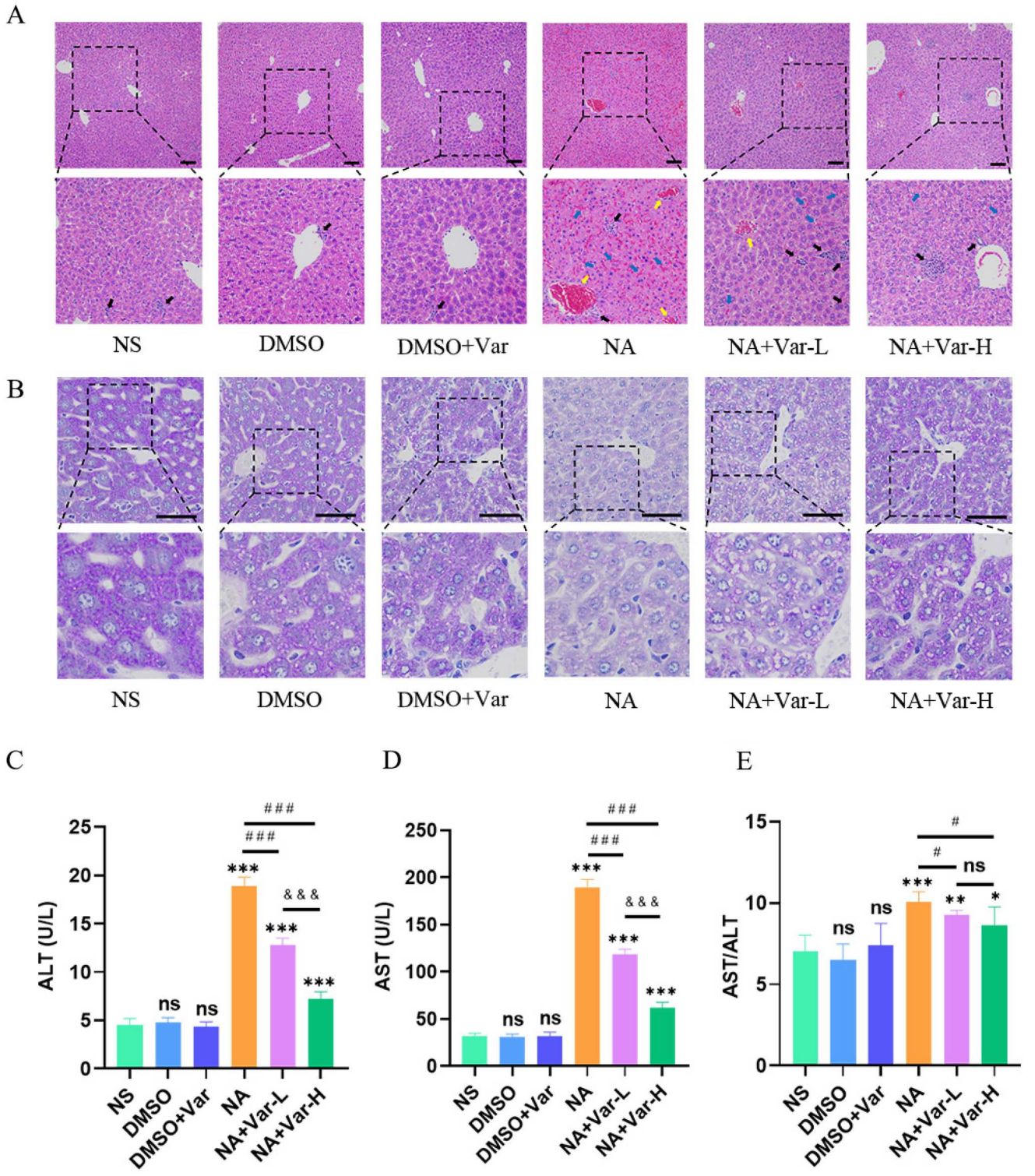

Figure 2. Varespladib effectively mitigates *N. atra*-induced ALI. (A) H&E staining was performed on liver tissue sections. Inflammatory cell infiltration is marked with a black arrow, liver sinus congestion is marked with blue arrows, and central venous congestion is marked with yellow arrows. (B) PAS staining of liver sections. (C–E) The liver function indicators. Scale bar, 100 μm. $^{*}p < 0.05$, $^{**}p < 0.01$, and $^{***}p < 0.001$ vs. NS group. $^{\#}p < 0.05$, $^{\#\#}p < 0.01$ and $^{\#\#\#}p < 0.001$ vs. NA group. $^{\&}p < 0.05$, $^{\&\&}p < 0.01$ and $^{\&\&\&}p < 0.001$ vs. NA + Var-L group. ns, not significant.

reflects the free energy distribution of the system, which was used to identify stable conformations and transition paths. In the 3D map of the FEL, the horizontal and vertical coordinates represent the principal components, and the color reflects the free energy size, the deeper the blue, the lower the free energy. The whole system is primarily distributed in two low-energy regions, confirming structural stability (Figure 5E–G). Overall, the MDS results suggest that $SVPLA_2$ stably binds to Nrf2, suggesting that Nrf2 may serve as a direct toxicity target of $SVPLA_2$.

To further validate the result of molecular docking and MDS, western blot analysis was performed in L02 cells. Compared to the NS group, *N. atra* venom significantly reduced the protein expression of Nrf2 and its downstream targets, including HO-1 and NQO-1, in L02 cells. However, varespladib effectively counteracted this effect by inhibiting PLA_2 (Figure 5H–K). The results of the Co-IP assay also confirmed that $SVPLA_2$ from *N. atra* venom can indeed interact with Nrf2 (Figure 5L). The above results further demonstrate $SVPLA_2$ targets Nrf2 to impair redox homeostasis.

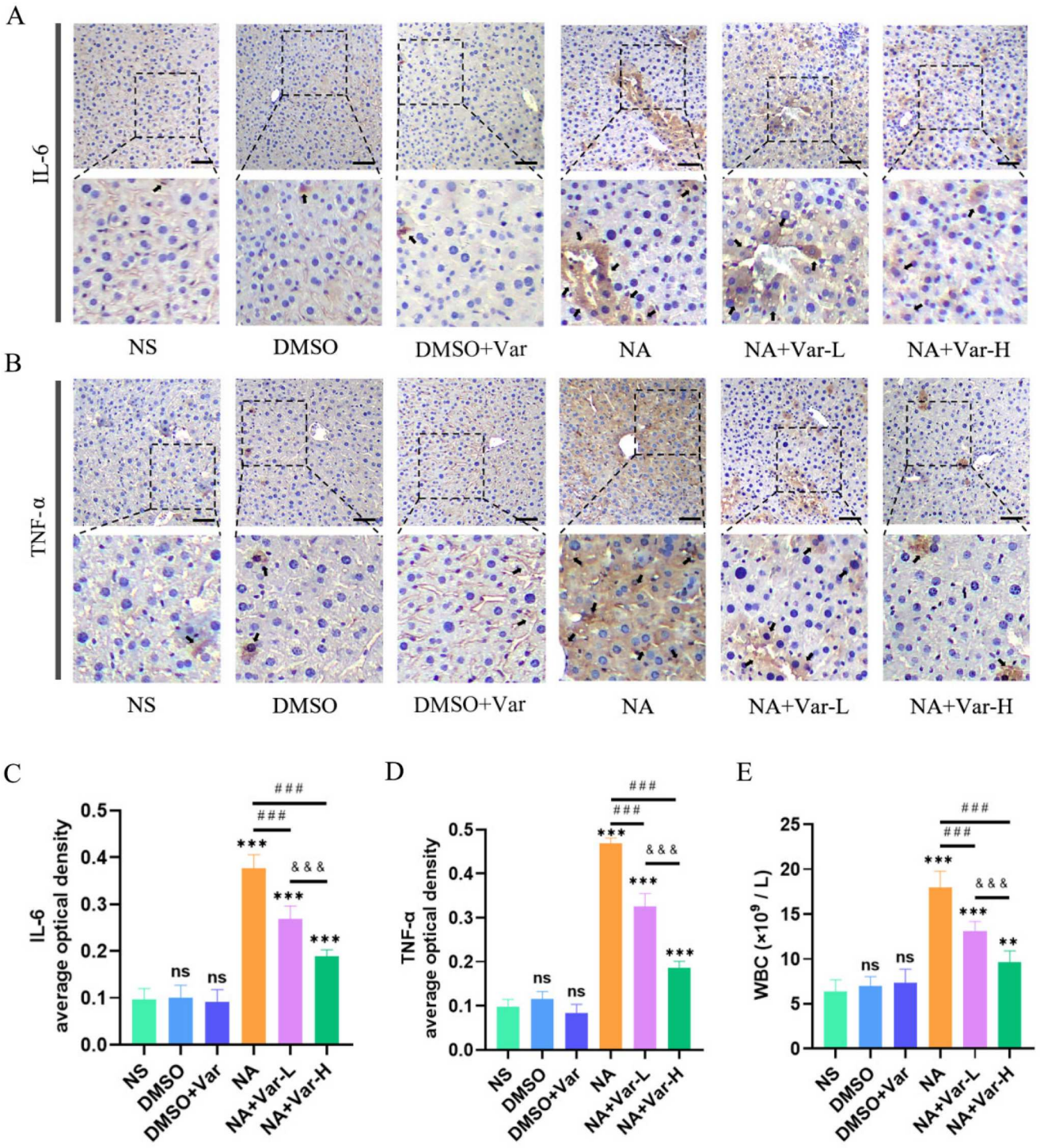

Figure 3. Varespladib alleviates *N. atra*-induced liver inflammation. (A–B) IHC was used to detect the expressions of inflammation factors in liver sections. (C–D) The quantification of the IHC images. (E) White blood cell count in a whole blood sample of each animal model group. Scale bar, 100 μm. $^{*}p < 0.05$, $^{**}p < 0.01$, and $^{***}p < 0.001$ vs. NS group. $^{\#}p < 0.05$, $^{\#\#}p < 0.01$ and $^{\#\#\#}p < 0.001$ vs. NA group. $^{\&}p < 0.05$, $^{\&\&}p < 0.01$ and $^{\&\&\&}p < 0.001$ vs. NA + Var-L group. ns, not significant.

3.5. Blockade of Nrf2 abolishes the hepatoprotective effects of varespladib

According to the results of the CCK-8 assay, the IC_{50} of *N. atra* venom against L02 cells was 117 μg/mL. Next, L02 cells were exposed to *N. atra* venom at the IC_{50} concentration to evaluate the protective effects of varespladib, the optimal varespladib dose was determined to be 180 μg/mL. Accordingly, *N. atra* venom was applied at 117 μg/mL, while varespladib was used at low (90 μg/mL) and high (180 μg/mL) doses in vitro experiments (Figure 6A and B).

Considering that $SVPLA_2$ can directly bind Nrf2 protein, we knocked down the Nrf2 expression in L02 cells using Nrf2 siRNA transfection to further elucidate the role of Nrf2 and its downstream mechanism in *N. atra* venom-induced oxidative stress. Western blot and qRT-PCR results indicated that the efficiency of Nrf2 knockdown was efficient, which can be used for subsequent experiments (Figure 6C and D). As expected, *N. atra* venom triggered significant oxidative stress, which was verified through oxidative stress markers and intracellular ROS levels (Figure 7). These effects were almost reversed by varespladib treatment. However, in Nrf2 knockdown cells, varespladib failed to exert its protective effects. These findings suggest that the serious oxidative stress observed in the liver of *N. atra* envenomed mice is

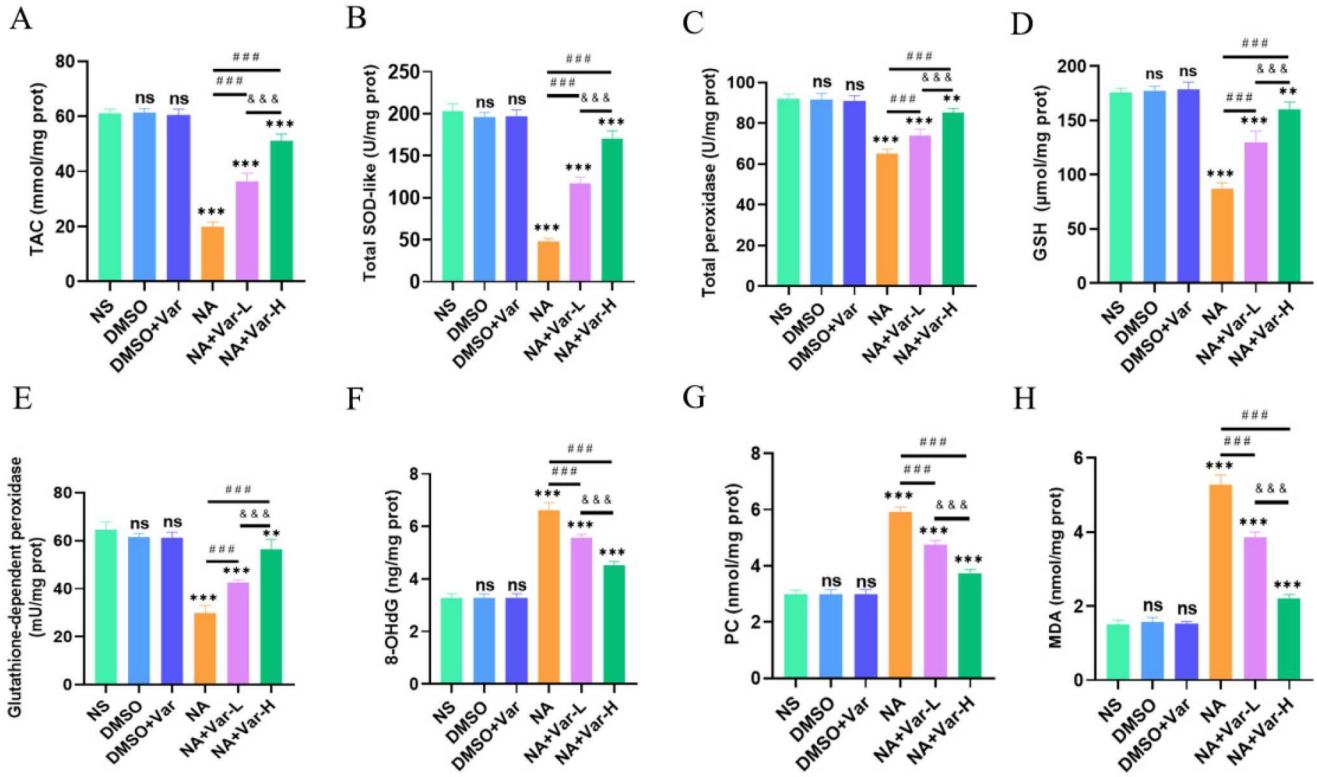

Figure 4. Varespladib treatment improves oxidative stress in the livers. (A–H) Detection of oxidative stress indicators in liver tissue. *$p < 0.05$, **$p < 0.01$, and ***$p < 0.001$ vs. NS group. $^{\#}p < 0.05$, $^{\#\#}p < 0.01$ and $^{\#\#\#}p < 0.001$ vs. NA group. $^{\&}p < 0.05$, $^{\&\&}p < 0.01$ and $^{\&\&\&}p < 0.001$ vs. NA + Var-L group. ns, not significant.

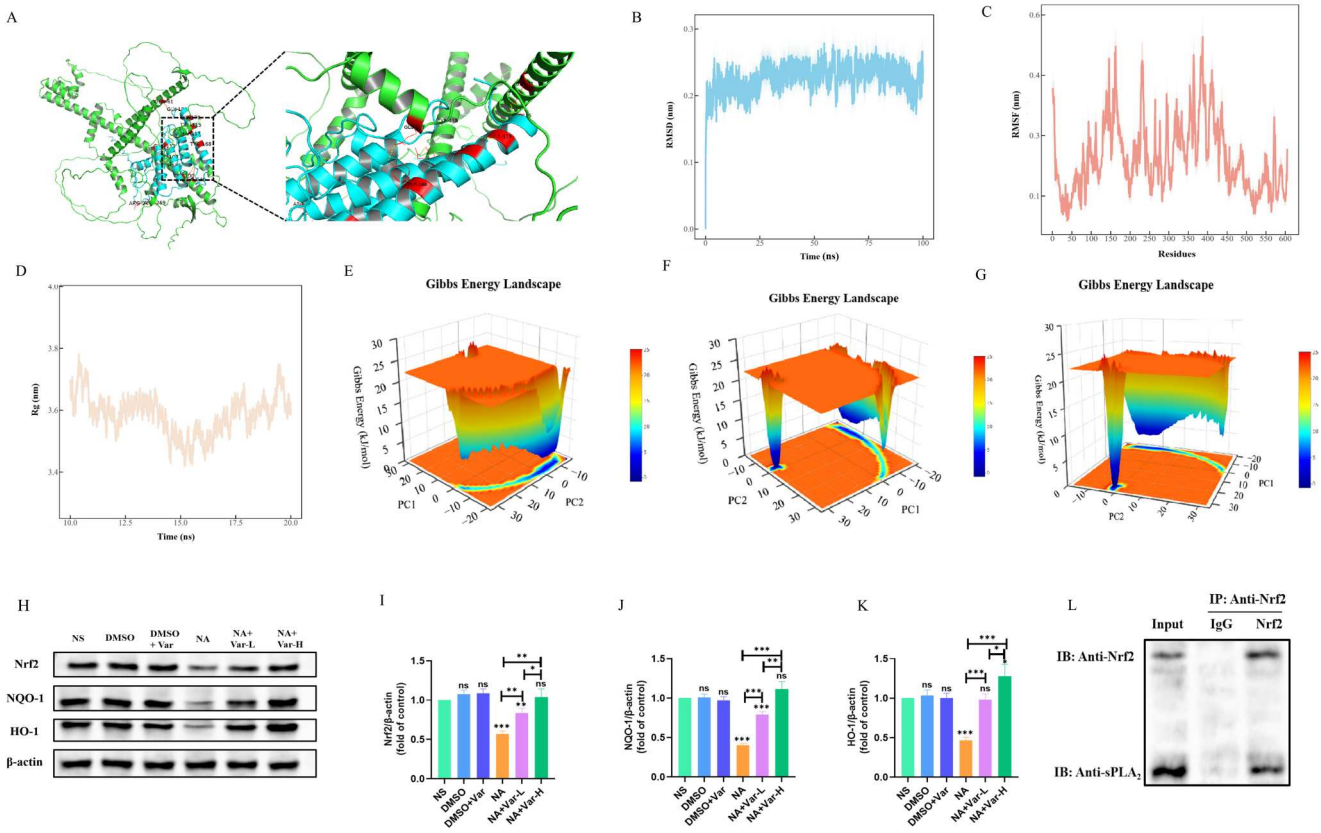

Figure 5. $SVPLA_2$ directly binds to Nrf2. (A) The interaction of $SVPLA_2$ with the Nrf2 protein in molecular docking analysis. (B–G) A 100-ns MDS between $SVPLA_2$ and Nrf2. (H) Protein levels of Nrf2, NQO-1 and HO-1 were measured by Western blot analysis in L02 cells, (I-K) and the quantitative maps were created. (L) Co-IP between $SVPLA_2$ and Nrf2. *$p < 0.05$, **$p < 0.01$, and ***$p < 0.001$. ns, not significant.

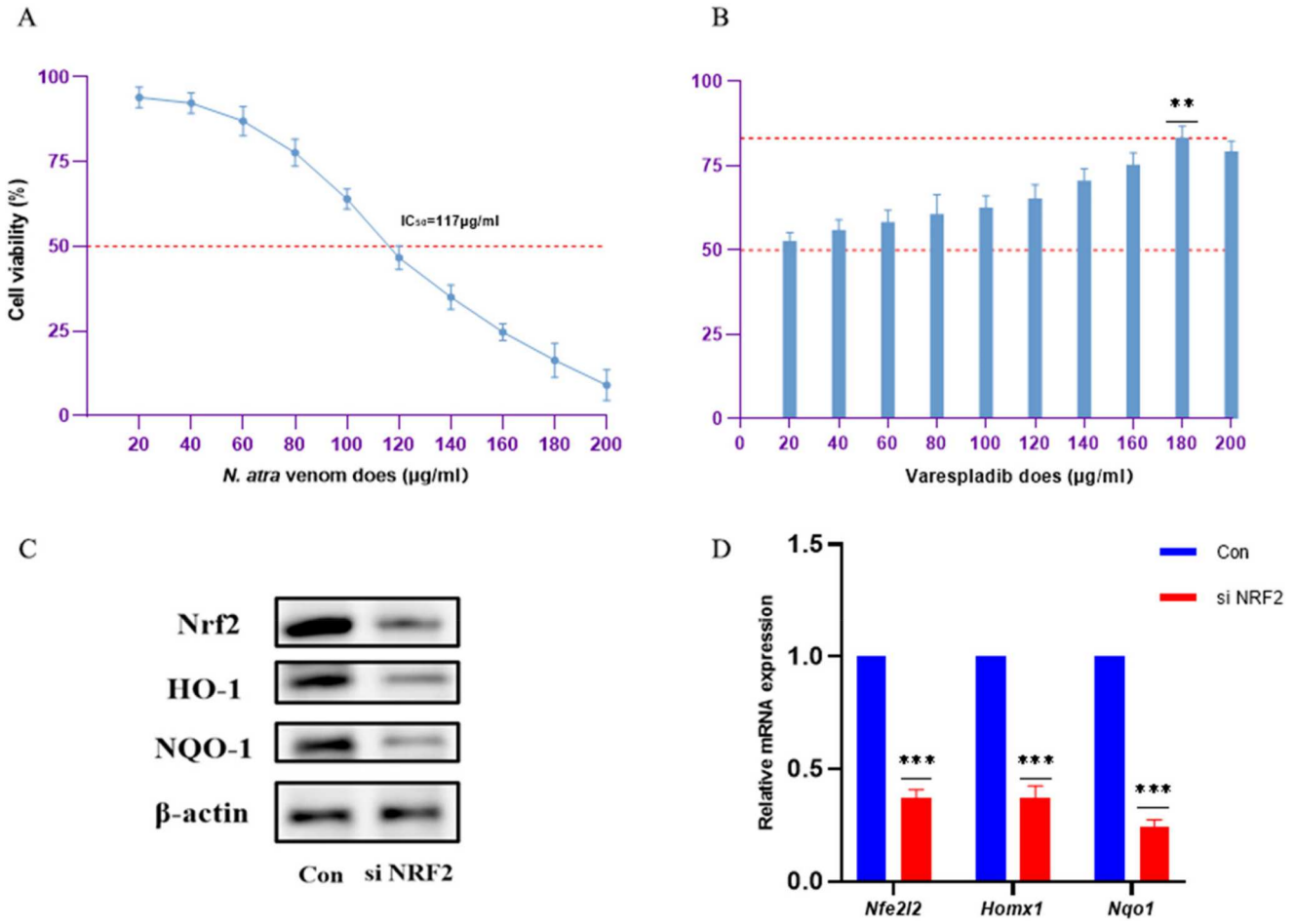

Figure 6. Cell viability assay and validation of the efficiency of Nrf2 knockdown. (A) Determination of the IC_{50} of *N.atra* venom on L02 cells (μg/mL); (B) Determination of the inhibitory concentration of Varespladib (μg/mL) against *N. atra* venom according to the *N.atra* venom IC_{50} value. (C–D) Validation of Nrf2 knockdown efficiency at protein level and mRNA level. *$p < 0.05$, **$p < 0.01$, and ***$p < 0.001$. ns, not significant.

mediated viaNrf2 signaling, and the hepatoprotective effects of varespladib are abolished when Nrf2 is blocked.

3.6. Varespladib reverses N. atra*-induced ferroptosis via Nrf2 signaling.*

Ferroptosis is an identified form of iron-dependent programmed cell death (PCD), regulated by GPX4 and lipid peroxidation [52,53]. Our results demonstrated that *N. atra* venom significantly induced lipid peroxidation and impaired glutathione-dependent peroxidase activity both in vivo and in vitro. Furthermore, liver iron levels in *N. atra*-treated mice were significantly elevated compared to the NS group, these changes were effectively reversed by varespladib (Figure 8A). Current research indicates that GPX4 expression is positively correlated with cellular resistance to ferroptosis [54], while ACSL4, an important isozyme in polyunsaturated fatty acid (PUFA) metabolism, increases susceptibility to ferroptosis by preferentially catalyzing PUFA such as AA [55]. Therefore, we evaluated the expression of GPX4 and ACSL4 following *N. atra* venom exposure. The results showed significant reduction in GPX4 levels and increase in ACSL4 levels in the liver tissue of *N. atra* envenomed mice, both of which were reversed by varespladib. Interestingly, varespladib's protective effect against *N. atra*-induced ferroptosis in L02 cells was lost upon Nrf2 gene knockdown (Figure 8B–D). These results suggest that *N. atra*-triggered ferroptosis is mediated via the Nrf2 signaling, and inhibition of PLA_2 could play a critical role in resisting ferroptosis.

3.7. Varespladib relieves N. atra*-induced mitochondrial dysfunction via Nrf2 signaling*

Mitochondrial dysfunction is regarded as another important event in animal toxin-caused cellular damage [37]. Numerous studies have shown that *N. atra* venom induces serious mitochondrial dysfunction, but the underlying mechanism remains unclear [19]. To evaluate the impacts of *N. atra* venom and varespladib on mitochondrial function, key indicators of mitochondrial homeostasis were measured. CS activity, a common marker of mitochondrial content, was significantly reduced following *N. atra* venom exposure, along with a decrease in ATP production (Figure 9A and B). Additionally, mitochondrial ROS were markedly elevated, further leading to impaired MMP (Figure 9C and D). CCCP, a mitochondrial uncoupling agent (positive control), directly disrupts the mitochondrial membrane potential. These results suggest that *N. atra* venom disrupts mitochondrial structure and function, while varespladib effectively protected L02 cells from these mitochondrial impairments. Importantly, the Nrf2 signaling was implicated in the mechanism, as varespladib failed to preserve mitochondrial homeostasis when Nrf2 was knocked down.

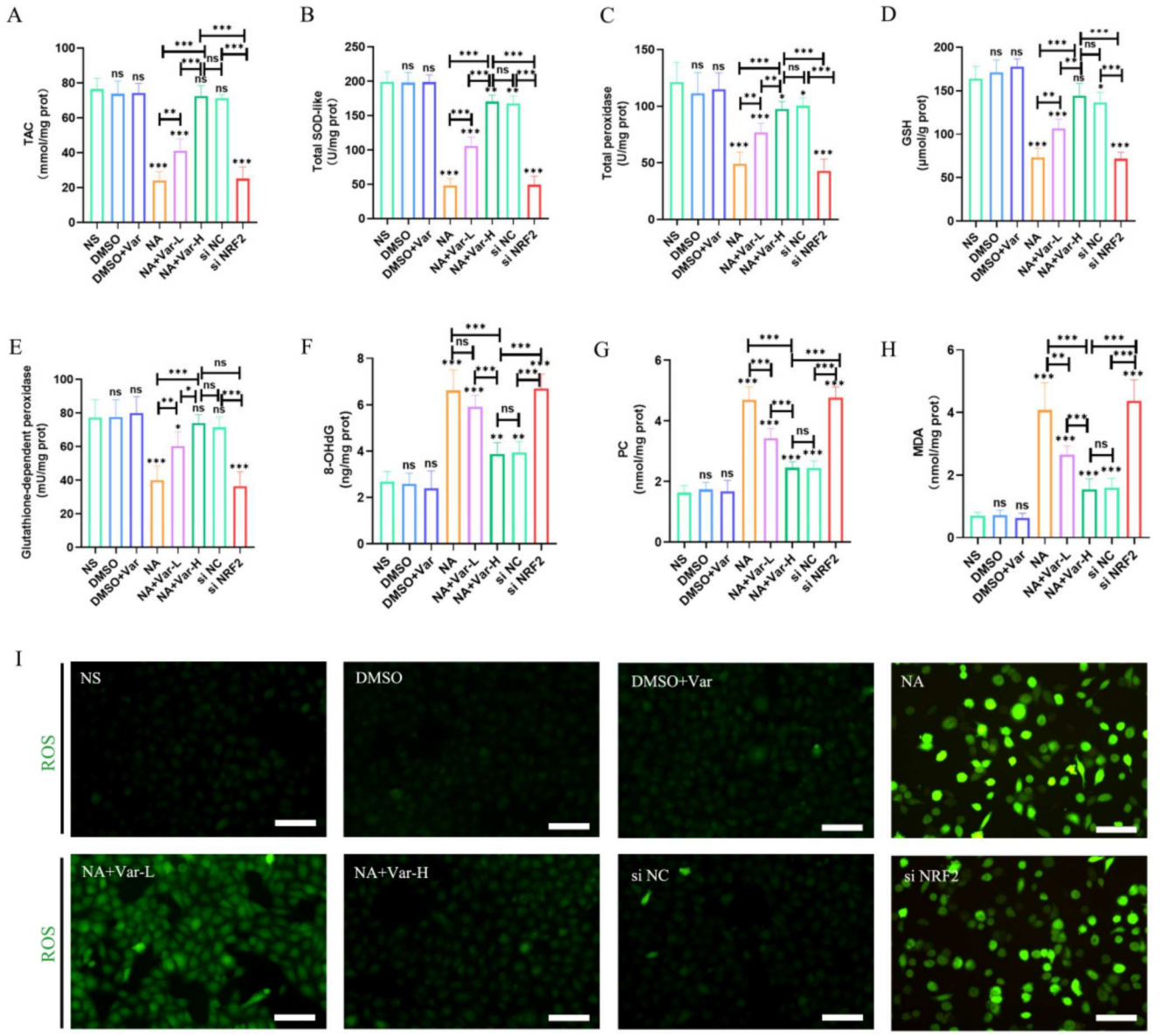

Figure 7. Varespladib relieves *N. atra* venom-induced oxidative stress in L02 cells. Blockade of Nrf2 abolishes the hepatoprotective effects of varespladib. (A-H) Detection of oxidative stress indicators in L02 cells. (I) The ROS content in L02 cells was determined by immunofluorescence. Scale bar, 100 μm. $^{*}p < 0.05$, $^{**}p < 0.01$, and $^{***}p < 0.001$. ns, not significant.

3.8. Varespladib suppresses N. atra*-induced excessive mitophagy via Nrf2 signaling*

Building on the previous findings, *N. atra* venom disrupts mitochondrial homeostasis, leading to the release of excessive mitochondrial ROS, a key initiation factor for mitophagy [19]. This study further examined the impacts of *N. atra* venom on mitophagy and the role of the Nrf2 signaling. Western blot analysis revealed that *N. atra* venom triggered excessive mitophagy, as evidenced by elevated expression of PINK1, Parkin, and LC3II/I in L02 cells. Varespladib, particularly in the Var-H group, effectively inhibited this excessive mitophagy. Similarly, the suppression of *N. atra*-induced mitophagy by varespladib was closely linked to the Nrf2 signaling (Figure 9E–H).

3.9. Varespladib inhibits N. atra*-induced mitochondria-mediated apoptosis via Nrf2 signaling.*

Mitochondrial dysfunction and abnormal mitophagy are frequently linked to mitochondria-mediated apoptosis [22,56]. Flow cytometry results showed a significant increase in the apoptotic rate in the NA group (Figure 10A). Western blotting analysis revealed that *N. atra* venom treatment led to an upregulation of Cleaved Caspase-9, Cleaved Caspase-3, and Bax, alongside a downregulation of the anti-apoptotic protein Bcl-2, further indicating the induction of apoptosis. In contrast, varespladib treatment significantly reduced apoptosis in L02 cells. Previous research has demonstrated that mitochondrial stress causes the release of Cyt c into the cytoplasm, subsequently activating Caspase-3 and Caspase-9, initiating apoptosis. Immunoblotting was employed to assess Cyt c levels in the cytoplasm, confirming that *N. atra* venom caused abnormal Cyt c release, which was dose-dependently reversed by varespladib. However, when the Nrf2 gene was knocked down, a high dose of varespladib failed to rescue the reduction in *N. atra*-induced apoptosis (Figure 10B–I). The above results indicate that *N. atra* venom triggers serious mitochondrial damage and further induces mitochondria-mediated apoptosis, and varespladib could protect L02 cells from *N. atra* venom, which is modulated by the Nrf2 signaling pathway.

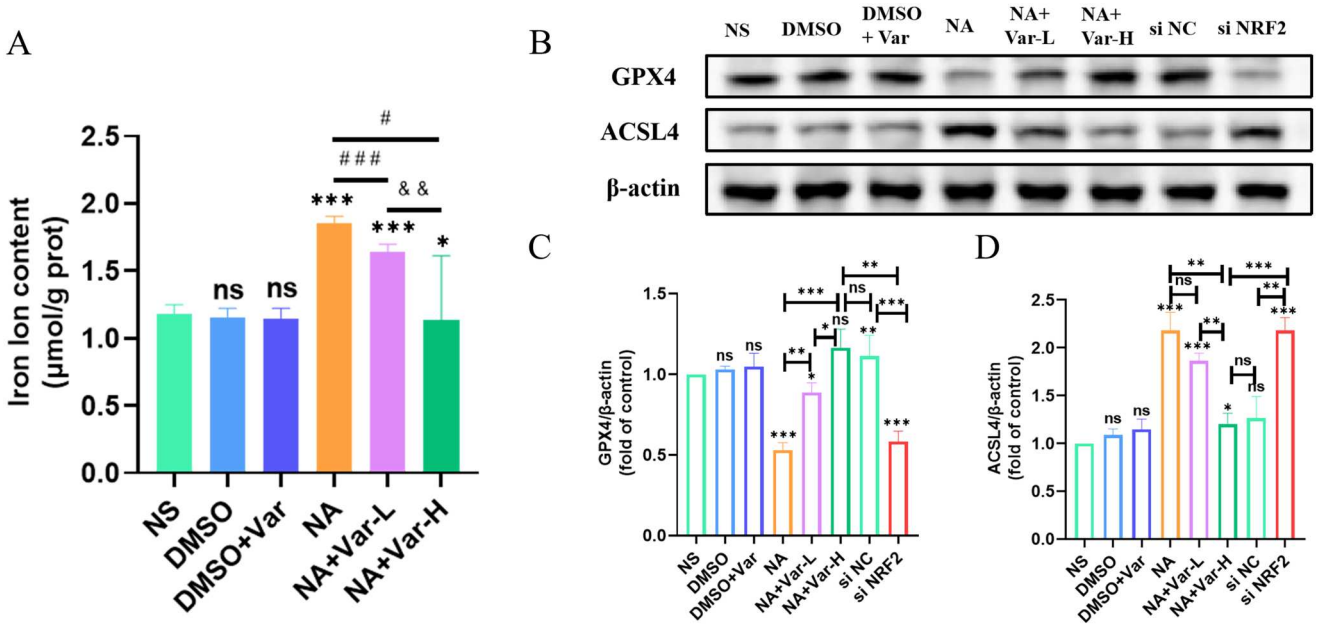

Figure 8. Varespladib reverses *N. atra*-induced ferroptosis via Nrf2 signaling. (A) Determination of iron ion content in liver tissue. (B) Protein levels of GPX4 and ACSL4 were measured by Western blot analysis in L02 cells, (C–D) and the quantitative maps were created. *$p < 0.05$, **$p < 0.01$, and ***$p < 0.001$. ns, not significant.

4. Discussion

Snakebite envenomations pose a huge threat to human safety, prompting the WHO to launch a global roadmap aimed at halving snakebite-related fatalities and disabilities by 2030 [57]. Achieving this task requires prioritizing research and treatment strategies. Varespladib, a small-molecule inhibitor, has gained increasing attention due to its protective effects against multiple snake venoms [40]. In this study, we evaluated the hepatoprotective effects of varespladib on *N. atra* venom-triggered ALI and identified the toxic target and pathomechanism of $SVPLA_2$.

Numerous studies have shown that organ injuries resulting from snakebite envenomation are comparable, with ALI being one of the most common complications [15–17]. As the primary detoxification organ, the liver is particularly susceptible to snake venom. This underscores the liver's vulnerability to venom-induced damage. ALI induced by *N. atra* venom is typically marked by significant elevations in liver function markers and notable histopathological alterations. Previous studies have suggested that targeting $SVPLA_2$ can alleviate these pathological changes, indicating that $SVPLA_2$ is a key mediator of *N. atra*-induced ALI [19,22]. In the present study, we observed severe histopathological changes following *N. atra* envenomation, consistent with prior reports, and found that varespladib effectively mitigated these effects in a dose-dependent manner. These findings reinforce the conclusion that $SVPLA_2$ is the primary toxic component of *N. atra* venom, and suggest that varespladib holds considerable therapeutic potential for treating snakebite envenomation through $SVPLA_2$ inhibition.

Moreover, snakebite envenomation commonly triggers acute and chronic inflammatory responses [58,59]. Nandana reported activation of the NLRP3 inflammasome in mouse macrophages following *Naja naja* envenomation, along with IL-1β production and Caspase-1 activation, both of which were blocked by NLRP3 inhibitors. Snake venom toxins, such as $SVPLA_2$ and SVMPs, have been implicated in promoting inflammatory responses through multiple signaling pathways, with PLA_2 being specifically shown to enhance inflammation via NLRP3 activation [50]. In this study, we also observed marked inflammatory responses in the liver of *N. atra*-envenomed mice, potentially linked to NLRP3 inflammasome activation or other inflammatory pathways, but further investigation is required to investigate the precise mechanisms involved.

Oxidative stress is widely recognized as a key event in snake toxin-induced cellular damage [22–25]. Clinical data from snakebite envenomation patients have shown decreased levels of TAC, SOD, and GSH, along with a significant increase in MDA [60]. Mechanistically, $SVPLA_2$ disrupts the electron transport chain, causing the production of mitochondrial ROS. This interaction induces oxidative stress, disrupts cell membranes, and exacerbates local tissue inflammation [61,62]. These results suggest that venom triggers serious oxidative stress, thereby worsening cellular damage. Fu et al. also demonstrated that several snake venoms can induce severe oxidative stress in snakebite-envenomed mice, with the toxic effects of *N. atra* and *Deinagkistrodon acutus* (Viperidae) venoms being the most pronounced [22]. Notably, inhibition of $SVPLA_2$ has been shown to alleviate snake venom – induced oxidative stress. Considering the disruptive effects of *N. atra* venom on redox homeostasis, we investigated oxidative stress in the liver tissue of the NA group, assessing both oxidative damage and antioxidant capacity. *N. atra* venom induced significant damage to lipids, DNA, and proteins, indicative of oxidative injury, whereas varespladib markedly attenuated this biomolecular damage. Consistently, *N. atra* exposure impaired the hepatic antioxidant system by reducing GSH levels and glutathione peroxidase activity, as further confirmed by in vitro experiments. These findings suggest that *N. atra* venom disrupts redox balance, while varespladib mitigates this effect through $SVPLA_2$ inhibition. Thus, maintaining redox homeostasis may represent a promising therapeutic approach for *N. atra*-induced liver injury, although the precise mechanisms warrant further investigation. However, it is important to

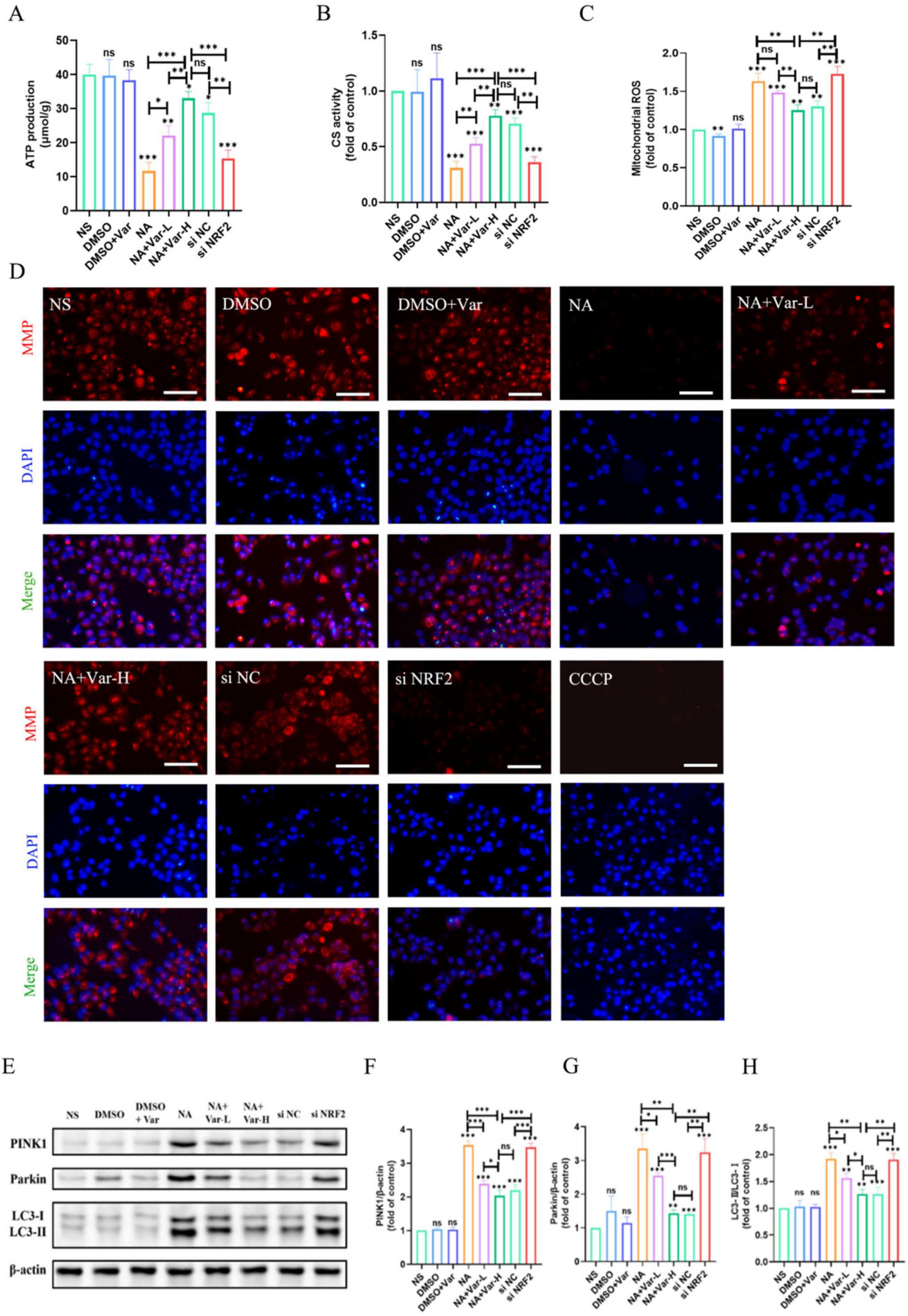

Figure 9. Varespladib relieves *N. atra*-induced mitochondrial dysfunction and suppresses *N. atra*-induced excessive mitophagy via Nrf2 signaling. (A) ATP production in L02 cells. (B) CS activity in L02 cells. (C) Mitochondrial ROS in L02 cells. (D) MMP in L02 cells. (E) Protein levels of PINK1, Parkin, and LC3-II/I were measured by Western blot analysis in L02 cells. (F–H) and the quantitative maps were created. *$p < 0.05$, **$p < 0.01$, and ***$p < 0.001$. ns, not significant.

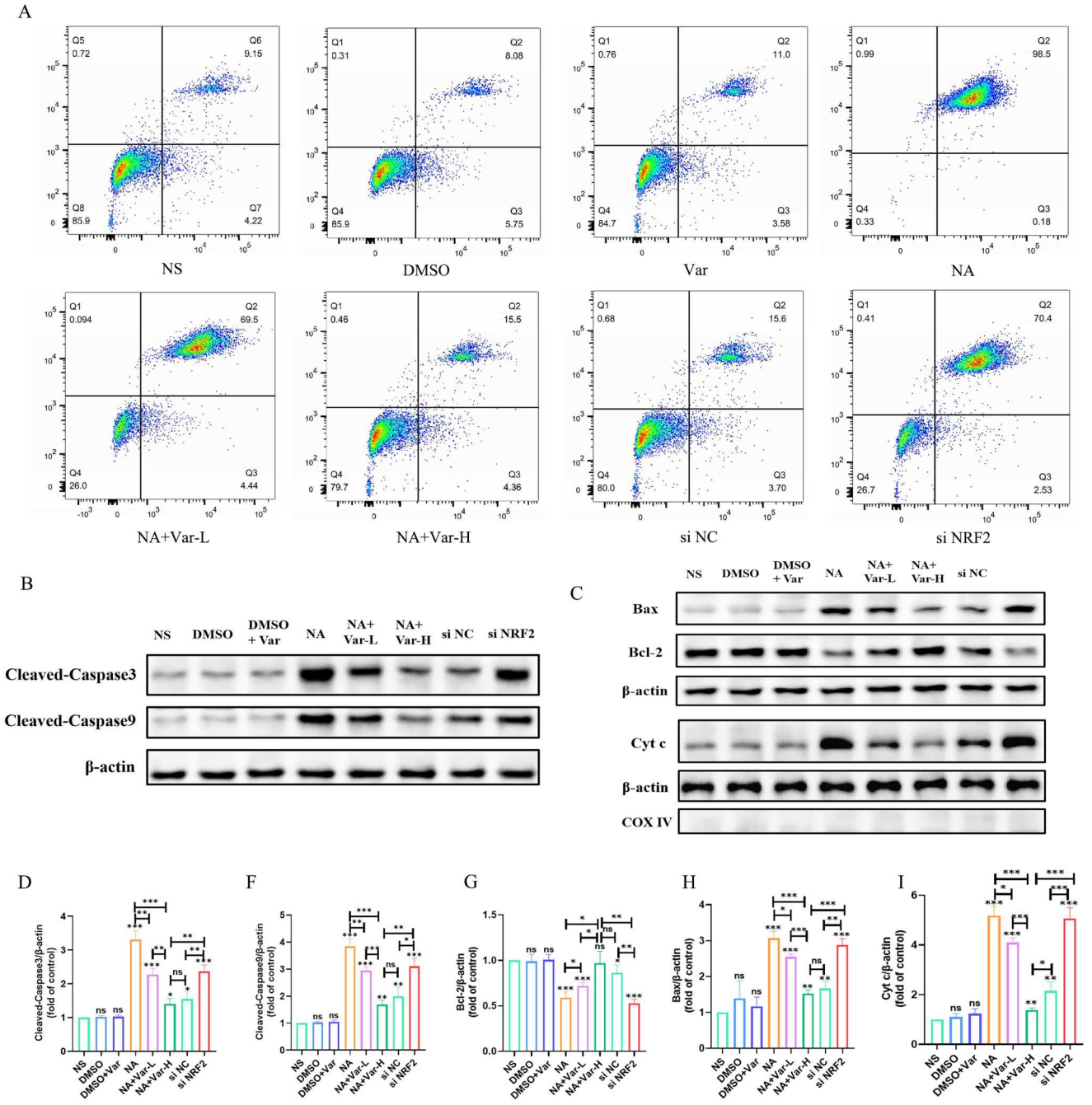

Figure 10. Varespladib inhibits *N. atra*-induced mitochondria-mediated apoptosis via Nrf2 signaling. (A) Apoptosis was detected by flow cytometry. (B) Protein levels of Cleaved-Caspase 9 and Cleaved-Caspase 3 were measured by Western blot analysis in L02 cells. (C) Protein levels of Cyt c, Bax, and Bcl-2 were measured by Western blot analysis in L02 cells. (D-I) The quantitative maps of proteins were created. *$p < 0.05$, **$p < 0.01$, and ***$p < 0.001$. ns, not significant.

acknowledge certain methodological limitations in our assessment of redox-related enzyme activities. Specifically, the enzymatic activity measurements of SOD, CAT, and GPx were conducted using commercial assay kits that do not include specific pharmacological inhibitors. As such, the observed activities likely reflect total SOD-like, peroxidase, and glutathione-dependent peroxidase activity, respectively, rather than the activity of individual enzymes alone. This lack of specificity may lead to an overestimation or misattribution of the contributions of specific enzymes to the overall antioxidant capacity. While these limitations do not detract from the observed trends in oxidative stress and the protective effects of varespladib, they highlight the need for more refined approaches, such as the use of specific enzyme inhibitors – in future studies to precisely delineate the roles of individual antioxidant enzymes.

Recent studies have demonstrated that Nrf2-activating compounds exhibit significant positive effects in the snakebite envenomations model. For instance, fractions from *Moringa oleifera* leaves, an effective Nrf2 activator, have been shown to mitigate snake venom-triggered histopathological damage and inflammation by enhancing Nrf2 expression [29,63]. These findings suggest that Nrf2 may be a potential therapeutic target for snakebite envenomations. In our study, molecular docking was conducted to explore the potential interaction between $SVPLA_2$ and Nrf2. In Western blotting analysis, *N. atra* venom significantly suppressed Nrf2 signaling, but varespladib effectively restored it. Knockdown of Nrf2 gene abolished the protective effects of varespladib, further confirming that the Nrf2 plays a critical role in its protective mechanism.

In addition to modulating the antioxidant response, Nrf2 also regulates the expression of genes involved in ferroptosis

[32,33]. Several studies have highlighted that animal toxins can induce ferroptosis through modulation of the Nrf2 pathway. For instance, Ni et al. demonstrated that wasp venom (*Vespa magnifica*) triggers ferroptosis by elevating lipid ROS levels via Nrf2 downregulation [64]. However, ferroptosis in snake venom-induced cell death has not been previously reported. Lipid peroxidation, a hallmark of various pathological conditions, is a critical driver of ferroptosis [65,66]. In this study, we observed abnormally elevated iron ion levels and MDA content, indicating severe lipid peroxidation in liver tissue of *N. atra*-envenomed mice. Furthermore, high ACSL4 expression is a well-established biomarker linked to increased sensitivity to ferroptosis [67]. Our results show that *N. atra* venom significantly upregulates ACSL4 expression.

Furthermore, GSH plays a crucial role in antioxidant defenses, which is utilized by GPX4 to reduce lipid peroxides to alcohol, a critical defense mechanism against ferroptosis. Our study demonstrated that *N. atra* venom markedly decreased GPX4 expression and GSH levels [68]. Interestingly, the transcription of many essential anti-ferroptotic genes is controlled by Nrf2 [32,67]. Similarly, knocking down the Nrf2 gene abolished the resistant effect of varespladib on ferroptosis in this study. Taken together, our study is the first to demonstrate that snake venom can induce cell death through mechanisms other than apoptosis and necrosis. Specifically, $SVPLA_2$ triggers ferroptosis in hepatocytes via the Nrf2 signaling.

In addition to ATP production, mitochondria are the key organelles to maintain the balance between oxidation and antioxidation [37]. Numerous studies have identified mitochondrial damage as an important and common event in snake toxin-induced cellular injury [16,19,35]. $sPLA_2$ which is derived from snake venom could disrupt mitochondrial function and structure. For instance, Šribar et al. demonstrated that $SVPLA_2$ targets Cyt c oxidase in neuronal mitochondria, impairing the electron transport chain and oxidative phosphorylation [69]. Consistent with these findings, our study observed that *N. atra* venom reduced mitochondrial content and ATP production in hepatic cells. Besides, studies also reported multiple snake venoms could impair mitochondrial function by altering membrane permeability and reducing MMP [19]. Similarly, in our study, *N. atra* venom significantly decreased MMP in hepatic cells, a disruption that was effectively mitigated by varespladib treatment. Previous studies have shown that snake venom-induced cellular damage is closely linked to autophagy, for example, Costal-Oliveira et al. reported that L-amino acid oxidase (LAAO) prevented keratinocyte formation through autophagy [70,71]. Mitophagy is a specific form of autophagy. In some cases, for example, ROS accumulation and inflammatory reactions, the mitochondria will be damaged. The cell will selectively recognize, wrap, and degrade these mitochondria to prevent further injury. PINK1 and Parkin, which drive the ubiquitination of mitochondrial surface proteins, are well-established biomarkers of mitophagy [72]. Under normal conditions, PINK1 enters the mitochondrial inner membrane; however, when MMP declines, PINK1 accumulates on the outer membrane, recruiting and activating Parkin [73]. The conformational change in Parkin triggers its E3 ubiquitin ligase activity, leading to the ubiquitination of mitochondrial outer membrane proteins. LC3 proteins next recognize these ubiquitin-tagged proteins, targeting the damaged mitochondria for degradation. Excessive activation of mitophagy can lead to the removal of healthy mitochondria, which is harmful to cells [74]. Zhao et al. have confirmed that $SVPLA_2$ from *N. atra* venom induces excessive mitophagy [19]. In the present study, *N. atra* venom was observed to induce severe mitochondrial dysfunction, resulting in excessive mitochondrial ROS release and further impairment of MMP, key triggers of mitophagy. We further investigated the role of mitophagy in this process. Our findings suggested that *N. atra* venom treatment significantly elevated PINK1 and Parkin levels, while varespladib treatment normalized these levels. Therefore, liver injury caused by *N. atra* venom may be linked to abnormal mitophagy. Notably, previous findings indicated that $SVPLA_2$ impairs redox homeostasis and induces oxidative stress by directly binding to Nrf2. Therefore, we further explored the role of Nrf2 in this process. Interestingly, the Nrf2 signaling pathway was implicated, as varespladib failed to maintain mitochondrial homeostasis and suppress excessive mitophagy when Nrf2 was knocked down.

Many investigations also have reported the relationship between snake venom and PCD, with autophagy being the type most associated with $sPLA_2$, as previously discussed [42]. Besides autophagy, apoptosis is another critical form of PCD linked to $sPLA_2$. For instance, $sPLA_2$ has been shown to induce AKI by complement-mediated mitochondrial apoptosis via the NF-κB pathway [75,76]. In our study, *N. atra* venom was observed to cause mitochondrial dysfunction, and varespladib could rescue this injury by inhibiting PLA_2, which is regulated by the Nrf2 signaling. Mitochondrial stress is a critical initial element that triggers mitochondrial-mediated apoptosis, and the results from flow cytometry further support this perspective. Abnormal cyt c release was also detected via Western blotting, suggesting that apoptosis is mediated by mitochondria. Notably, $SVPLA_2$ from *N. atra* venom induced mitochondrial-mediated apoptosis, which was modulated by the Nrf2 signaling pathway. However, further investigations are warranted to explore whether *N. atra* venom can induce apoptosis through the extrinsic death receptor pathway or other forms of PCD, thereby providing additional insights into the pathophysiology of snake toxins and potential clinical applications.

5. Conclusions

This study systematically evaluates the hepatoprotective effects of varespladib against ALI induced by *N. atra* venom and investigates the mechanisms by which $SVPLA_2$ triggers hepatic oxidative stress through the Nrf2 signaling and its downstream pathways. The results indicate that varespladib mitigates ALI triggered by *N. atra* venom and inflammatory responses. The mechanism of $SVPLA_2$-induced oxidative stress is associated with the Nrf2 signaling. Specifically, $SVPLA_2$ can directly bind to the Nrf2 protein, inducing oxidative stress, which further triggers ferroptosis and impairs mitochondrial homeostasis, eventually leading to excessive mitophagy and mitochondrial-mediated apoptosis. Notably, these effects can be reversed by varespladib via the inhibition of PLA_2. Figure 11 shows the overall mechanism diagram of this paper. Taken together, this study suggests that varespladib serves as a promising PLA_2 inhibitor with potential therapeutic implications for treating snakebite envenomation, and Nrf2 is identified as a direct toxicity target of $SVPLA_2$, with

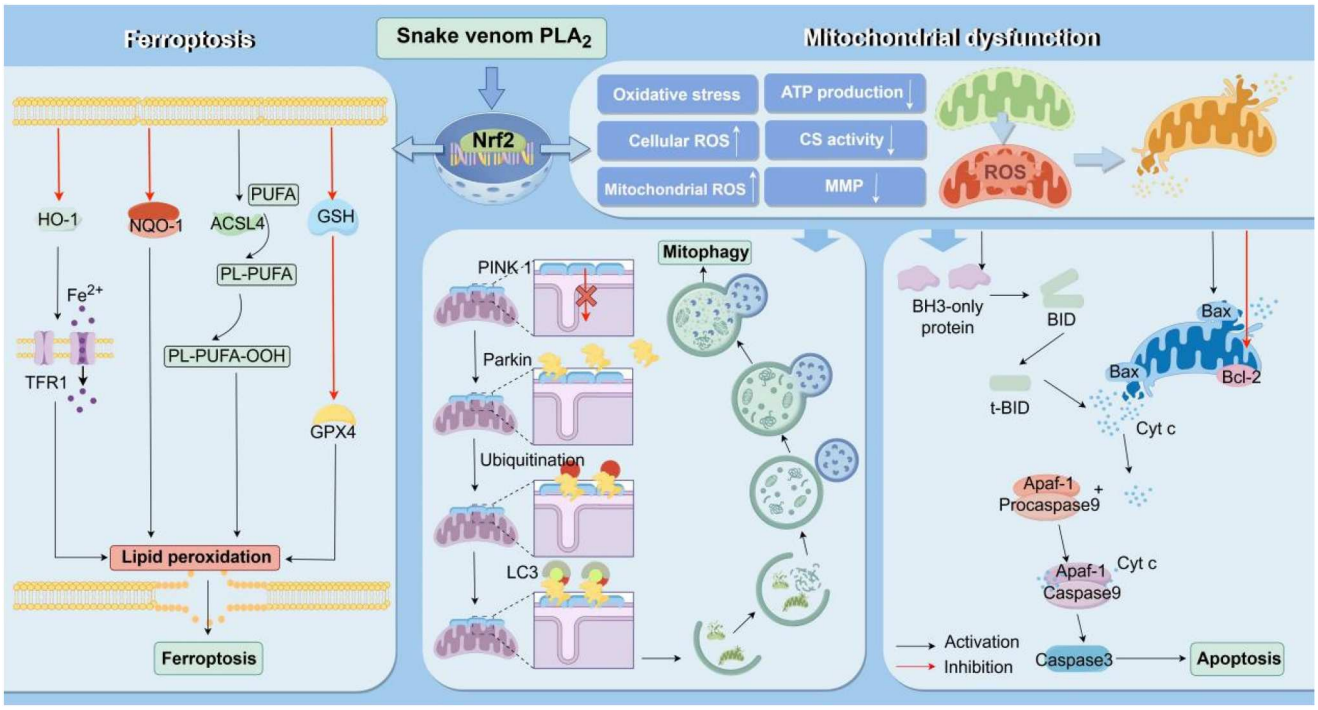

Figure 11. Schematic representation of $SVPLA_2$ target Nrf2 trigger ferroptosis and mitochondrial dysfunction (By Figdraw).

Nrf2-mediated ferroptosis and mitochondrial dysfunction playing critical roles in the toxic mechanism of $SVPLA_2$.

Acknowledgements

Thanks to GenProX for their work on molecular dynamics simulation. Thanks to Jingjin Wu, Yaoxing Wei, Na Li and Kunpeng Jiang for their guidance in the experiment.

Author contributions

CRediT: **Jiahao Liu:** Conceptualization, Methodology, Writing – original draft; **Linfeng Wang:** Writing – original draft; **Mengxia Xie:** Investigation; **Wenjie Zhao:** Methodology; **Jiaqi Sun:** Writing – original draft; **Yuji Jin:** Supervision; **Meiling Liu:** Project administration; **Jianqi Zhao:** Formal analysis; **Lixia Cheng:** Validation; **Lixia Cheng:** Validation; **Lixia Cheng:** Validation; **Lixia Cheng:** Validation; **Lixia Cheng:** Validation; **Cheng Wen:** Writing – review & editing; **Xiaowen Bi:** Supervision; **Chunhong Huang:** Resources, Writing – review & editing.

Disclosure statement

No potential conflict of interest was reported by the author(s).

Funding

This work was supported by funding from the National Natural Science Foundation of China [grant numbers 32260135, 31960199], the Key Project of Natural Science Foundation of Jiangxi Province [grant number 20232ACB206063], the Natural Science Fund Program of Science and Technology Department of Jilin [grant number 20220101329JC], the Innovation Project of College Students in Jilin Province [grant number S202313706036] and the Innovation Project of Jilin Medical College Students [grant number 2024CXXL014].

Data availability statement

The data that support the findings of this study are available from the corresponding author, [C. Huang], upon reasonable request.

References

[1] Warrell DA. Snake bite. Lancet. 2010;375(9708):77–88. doi:10.1016/S0140-6736(09)61754-2
[2] Naik SB. Intravenous snake bite: A catastrophic snake envenomation. Ann Afr Med. 2023;22(3):239–245. doi:10.4103/aam.aam_9_23
[3] Bawaskar HS, Bawaskar PH, Bawaskar PH. The global burden of snake bite envenoming. J R Coll Physicians Edinb. 2021;51(1):7–8. doi:10.4997/JRCPE.2021.102
[4] Bhargava S, Kumari K, Sarin RK, et al. First-hand knowledge about snakes and snake-bite management: an urgent need. Nagoya J Med Sci. 2020;82(4):763–774. doi:10.18999/nagjms.82.4.763
[5] Mao YC, Liu PY, Chiang LC, et al. Naja atra snakebite in Taiwan. Clin Toxicol. 2018;56(4):273–280. doi:10.1080/15563650.2017.1366502
[6] Kumar TK, Lee Cs Fau - Yu C, Yu C. A case study of cardiotoxin III from the Taiwan cobra (Naja naja atra). Solution structure and other physical properties. Adv Exp Med Biol. 1996;391:115–129. doi:10.1007/978-1-4613-0361-9_7
[7] Almeida JR, Resende LM, Watanabe RK, et al. Snake venom peptides and low mass proteins: molecular tools and therapeutic agents. Curr Med Chem. 2017;24(30):3254–3282. doi:10.2174/0929867323666161028155611
[8] Sales TA, Marcussi S, Ramalho TC. Current anti-inflammatory therapies and the potential of secretory phospholipase A2 inhibitors in the design of New anti-inflammatory drugs: a review of 2012 - 2018. Curr Med Chem. 2020;27(3):477–497. doi:10.2174/0929867326666190201120646
[9] Sampat GH, Hiremath K, Dodakallanavar J, et al. Unraveling snake venom phospholipase A(2): an overview of its structure, pharmacology, and inhibitors. Pharmacol Rep. 2023;75(6):1454–1473. doi:10.1007/s43440-023-00543-8
[10] Hiu JJ, Yap MKK. Cytotoxicity of snake venom enzymatic toxins: phospholipase A2 and l-amino acid oxidase. Biochem Soc Trans. 2020;48(2):719–731. doi:10.1042/BST20200110
[11] Khan SA, Ilies MA-OX. The phospholipase A2 superfamily: structure, isozymes, catalysis, physiologic and pathologic roles. Int J Mol Sci. 2023;24(2):1353. doi:doi.org/10.3390ijms24021353.
[12] Benati RB, Costa TR, Cacemiro MDC, et al. Cytotoxic and pro-apoptotic action of MjTX-I, a phospholipase A2 isolated from Bothrops moojeni snake venom, towards leukemic cells. J Venom Anim Toxins Incl Trop Dis. 2018;24:40. doi:10.1186/s40409-018-0180-9
[13] Lomonte B, Rangel J. Snake venom Lys49 myotoxins: from phospholipases A(2) to non-enzymatic membrane disruptors. Toxicon. 2012;60(4):520–530. doi:10.1016/j.toxicon.2012.02.007

[14] Bickler PE, Abouyannis MA-O, Bhalla A, et al. Neuromuscular weakness and paralysis produced by snakebite envenoming: mechanisms and proposed standards for clinical assessment. Toxins (Basel). 2023;15(1):49. doi:10.3390/toxins15010049
[15] Asmari A, Khan Ha Fau - Manthiri AK, Manthiri Ra Fau - Al Yahya RA, et al. Effects of Echis pyramidum snake venom on hepatic and renal antioxidant enzymes and lipid peroxidation in rats. J Biochem Mol Toxicol. 2014;28(9):407–412. doi:doi.org/10.1002jbt.21578.
[16] Cano-Sanchez M, Ben-Hassen K, Louis OP, et al. Bothrops lanceolatus snake venom impairs mitochondrial respiration and induces DNA release in human heart preparation. PLoS Negl Trop Dis. 2022;16(6):e0010523. doi:10.1371/journal.pntd.0010523
[17] Albuquerque P, Mota SM. Snakebite-associated kidney injury. Contrib Nephrol. 2021;199:244–251. doi:10.1159/000517725
[18] Khimmaktong W, Nuanyaem N, Lorthong N, et al. Histopathological changes in the liver, heart and kidneys following Malayan pit viper (Calloselasma rhodostoma) envenoming and the neutralising effects of hemato polyvalent snake antivenom. Toxins (Basel). 2022;14(9):601. doi:10.3390/toxins14090601
[19] Zhao W, Liu J, Wang S, et al. Varespladib mitigates acute liver injury via suppression of excessive mitophagy on Naja atra envenomed mice by inhibiting PLA(2). Toxicon. 2024;242:107694. doi:10.1016/j.toxicon.2024.107694
[20] Bonilla-Aldana DK, Bonilla-Aldana JL, Ulloque-Badaracco JR, et al. Snakebite-associated infections: a systematic review and meta-analysis. Am J Trop Med Hyg. 2024;110(5):874–886. doi:10.4269/ajtmh.23-0278
[21] Pałgan K, Kuźmiński A, Janik A, et al. Snake (Vipera berus) bite: the cause of severe anaphylactic shock and hepatocellular injury. Int J Immunopathol Pharmacol. 2015;28(1):119–121. doi:10.1177/0394632015572566
[22] Fu K, Zhao J, Zhong L, et al. Dual therapy with phospholipase and metalloproteinase inhibitors from Sinonatrix annularis alleviated acute kidney and liver injury caused by multiple snake venoms. Biomed Pharmacother. 2024;177:116967. doi:10.1016/j.biopha.2024.116967
[23] Dias, D. A., Souza de Souza, K. F., Moslaves, I. S. B., et al. Identification of purinergic system components in the venom of Bothrops mattogrossensis and the inhibitory effect of specioside extracted from Tabebuia aurea. Purinerg Signal. 2024;21(2), 317–329. doi:10.1007/s11302-024-10032-z
[24] Rayapati AM, Vemulapati B, Fau - Chanda C, et al. Cobra (Naja naja) venom L-amino acid oxidase (NNLAAO70) induces apoptosis and secondary necrosis in human lung epithelial cancer cells. J Biosci. 2024;49:43. doi:10.1007/s12038-024-00429-8
[25] Polloni L, Costa TR, Morais LP, et al. Oxidative stress induced by Pollonein-LAAO, a new L-amino acid oxidase from Bothrops moojeni venom, prompts prostate tumor spheroid cell death and impairs the cellular invasion process in vitro. Cell Signal. 2023;109:110785. doi:10.1016/j.cellsig.2023.110785
[26] Kaspar JW, Niture Sk Fau - Jaiswal AK, Jaiswal AK. Nrf2:INrf2 (Keap1) signaling in oxidative stress. Free Radical Biol Med. 2009;47(9):1304–1309. doi:10.1016/j.freeradbiomed.2009.07.035
[27] Theodore M, Kawai Y, Fau - Yang J, et al. Multiple nuclear localization signals function in the nuclear import of the transcription factor Nrf2. J Biol Chem. 2008;283(14):8984–8994. doi:10.1074/jbc.M709040200
[28] Krajka-Kuźniak V, Paluszczak J, Baer-Dubowska W. The Nrf2-ARE signaling pathway: an update on its regulation and possible role in cancer prevention and treatment. Pharmacol Rep. 2017;69(3):393–402. doi:10.1016/j.pharep.2016.12.011
[29] Tao T, Zhang F, Chai L, et al. Effect of Agkistrodon acutus venom (AAVC-I) on apoptosis through modulation of the Keap1/Nrf2 pathway in HSC-3 oral squamous cell carcinoma cells. Transl Cancer Res. 2024;13(8):4341–4353. doi:10.21037/tcr-24-182
[30] Zhang W, Geng X, Dong Q, et al. Crosstalk between autophagy and the Keap1-Nrf2-ARE pathway regulates realgar-induced neurotoxicity. J Ethnopharmacol. 2023;301:115776. doi:10.1016/j.jep.2022.115776
[31] Adeyi AO, Ajisebiola BS, Adeyi OE, et al. Moringa oleifera leaf fractions attenuated Naje haje venom-induced cellular dysfunctions via modulation of Nrf2 and inflammatory signalling pathways in rats. Biochem Biophys Rep. 2021;25:100890. doi:10.1016/j.bbrep.2020.100890
[32] Ma H, Xing C, Wei H, et al. Berberine attenuates neuronal ferroptosis via the AMPK-NRF2-HO-1-signaling pathway in spinal cord-injured rats. Int Immunopharmacol. 2024;142(Pt B):113227. doi:10.1016/j.intimp.2024.113227
[33] Xue S, Chen H, Zhang J, et al. Qishen granule alleviates doxorubicin-induced cardiotoxicity by suppressing ferroptosis via nuclear erythroid factor 2-related factor 2 (Nrf2) pathway. J Ethnopharmacol. 2024;335:118604. doi:10.1016/j.jep.2024.118604
[34] Fan Q, Chang H, Tian L, et al. Methane saline suppresses ferroptosis via the Nrf2/HO-1 signaling pathway to ameliorate intestinal ischemia-reperfusion injury. Redox Rep. 2024;29(1):2373657. doi:10.1080/13510002.2024.2373657
[35] Rigoni M, Paoli M, Fau - Milanesi E, et al. Snake phospholipase A2 neurotoxins enter neurons, bind specifically to mitochondria, and open their transition pores. J Biol Chem. 2008;283(49):34013–34020. doi:10.1074/jbc.M803243200
[36] Ivanušec AA-O, Šribar JA-O, Leonardi AA-O, et al. Rat group IIA secreted phospholipase A(2) binds to cytochrome c oxidase and inhibits Its activity: A possible episode in the development of Alzheimer's disease. Int J Mol Sci. 2022;23(20):12368. doi:10.3390/ijms232012368
[37] Trefts E, Gannon M, Wasserman DH. The liver. Curr Biol. 2017;27(21):R1147–R1151. doi:10.1016/j.cub.2017.09.019
[38] Scheske L, Ruitenberg J, Bissumbhar B. Needs and availability of snake antivenoms: relevance and application of international guidelines. Int J Health Policy Manag. 2015;4(7):447–457. doi:10.15171/ijhpm.2015.75
[39] Di Fabio JL, Cortés Castillo M, Griffiths E. Landscape of research, production, and regulation in venoms and antivenoms: a bibliometric analysis. Pan Am J Pub Heal. 2021;45:e55. doi:10.26633/RPSP.2021.55
[40] Albulescu LO, Xie C, Ainsworth S, et al. A therapeutic combination of two small molecule toxin inhibitors provides broad preclinical efficacy against viper snakebite. Nat Commun. 2020;11(1):6094. doi:10.1038/s41467-020-19981-6
[41] Lewin MA-O, Carter RA-O, Matteo IA, et al. Varespladib in the treatment of snakebite envenoming: development history and preclinical evidence supporting advancement to clinical trials in patients bitten by venomous snakes. Toxins (Basel). 2022;14(11):783. doi:10.3390/toxins14110783
[42] Sun J, Liu J, Liu M, et al. New perspective for pathomechanism and clinical applications of animal toxins: programmed cell death. Toxicon. 2024;249:108071. doi:10.1016/j.toxicon.2024.108071
[43] Xiong S, Luo Y, Zhong L, et al. Investigation of the inhibitory potential of phospholipase A(2) inhibitor gamma from Sinonatrix annularis to snake envenomation. Toxicon. 2017;137:83–91. doi:10.1016/j.toxicon.2017.07.019
[44] Wang Y, Zhang J, Zhang D, et al. Exploration of the inhibitory potential of varespladib for snakebite envenomation. Molecules. 2018;23(2):391. doi:10.3390/molecules23020391
[45] Ilatovskaya DV, Blass G, Palygin O, et al. A NOX4/TRPC6 pathway in podocyte calcium regulation and renal damage in diabetic kidney disease. J Am Soc Nephrol. 2018;29(7):1917–1927. doi:10.1681/ASN.2018030280
[46] Hsu JT, Le PH, Lin CJ, et al. Mechanism of salutary effects of melatonin-mediated liver protection after trauma-hemorrhage: p38 MAPK-dependent iNOS/HIF-1α pathway. Am J Physiol. 2017;312(5):G427–G433. doi:10.1152/ajpgi.00440.2016
[47] Singh A, Copeland MM, Kundrotas PJ, et al. GRAMM web server for protein docking. Methods Mol Biol. 2024;2714:101–112. doi:10.1007/978-1-0716-3441-7_5
[48] Wang Y, Fan Z, Yang M, et al. Protective effects of E Se tea extracts against alcoholic fatty liver disease induced by high fat/alcohol diet: In vivo biological evaluation and molecular docking study. Phytomedicine. 2022;101:154113. doi:10.1016/j.phymed.2022.154113
[49] Zhou Y, Tang S, Chen T, et al. Structure-based pharmacophore modeling, virtual screening, molecular docking and biological evaluation for identification of potential poly (ADP-ribose) polymerase-1 (PARP-1) inhibitors. Molecules. 2019;24(23):4258. doi:10.3390/molecules24234258
[50] Nandana MB, Bharatha M, Vishwanath BS, et al. Naja naja snake venom-induced local toxicities in mice is by inflammasome activation. Toxicon. 2024;238:107590. doi:10.1016/j.toxicon.2023.107590

[51] Qiao X, Wu X, Chen S, et al. Discovery of novel and potent dual-targeting AXL/HDAC2 inhibitors for colorectal cancer treatment via structure-based pharmacophore modelling, virtual screening, and molecular docking, molecular dynamics simulation studies, and biological evaluation. J Enzyme Inhib Med Chem. 2024;39(1):2295241. doi:10.1080/14756366.2023.2295241
[52] Chen T, Shi R, Suo Q, et al. Progranulin released from microglial lysosomes reduces neuronal ferroptosis after cerebral ischemia in mice. J Cereb Blood Flow Metab. 2023;43(4):505–517. doi:10.1177/0271678X221145090
[53] Friedmann Angeli JA-O, Krysko DA-O, Conrad MA-O. Ferroptosis at the crossroads of cancer-acquired drug resistance and immune evasion. Nat Rev Cancer. 2019;19(7):405–414. doi:10.1038/s41568-019-0149-1
[54] Yang WS, SriRamaratnam R, Welsch ME, et al. Regulation of ferroptotic cancer cell death by GPX4. Cell. 2014;156(1-2):317–331. doi:10.1016/j.cell.2013.12.010
[55] Zhu L, Feng Z, Zhang J, et al. MicroRNA-27a regulates ferroptosis through SLC7A11 to aggravate cerebral ischemia-reperfusion injury. Neurochem Res. 2023;48(5):1370–1381. doi:10.1007/s11064-022-03826-3
[56] Cheng J, Wang Q, Li C, et al. Microanatomical investigation of the subtemporal transtentorial approach. J Sich Univ. Medical science edition. 2024;55(2):290–296. doi:10.12182/20240360506
[57] Williams DA-O, Faiz MA, Abela-Ridder B, et al. Strategy for a globally coordinated response to a priority neglected tropical disease: snakebite envenoming. PLoS Negl Trop Dis. 2019;13(2):e0007059. doi:10.1371/journal.pntd.0007059
[58] Paloschi MV, Boeno CN, Lopes JA, et al. Reactive oxygen species-dependent-NLRP3 inflammasome activation in human neutrophils induced by l-amino acid oxidase derived from Calloselasma rhodostoma venom. Life Sci. 2022;308:120962. doi:10.1016/j.lfs.2022.120962
[59] Luo P, Ji Y, Liu X, et al. Affected inflammation-related signaling pathways in snake envenomation: A recent insight. Toxicon. 2023;234:107288. doi:10.1016/j.toxicon.2023.107288
[60] Sunitha K, Hemshekhar M, Thushara RM, et al. Inflammation and oxidative stress in viper bite: an insight within and beyond. Toxicon. 2015;98:89–97. doi:10.1016/j.toxicon.2015.02.014
[61] Nethery D, Callahan La Fau - Stofan D, Stofan D, et al. PLA(2) dependence of diaphragm mitochondrial formation of reactive oxygen species. J Appl Physiol. 2000;89(1):72–80. doi:10.1152/jappl.2000.89.1.72
[62] Lambert IH, Pedersen Sf Fau - Poulsen KA, Poulsen KA. Activation of PLA2 isoforms by cell swelling and ischaemia/hypoxia. Acta Physiol. 2006;187(1-2):75–85. doi:10.1111/j.1748-1716.2006.01557.x
[63] Adeyi AO, Adeyemi SO, Effiong EP, et al. Moringa oleifera extract extenuates echis ocellatus venom-induced toxicities, histopathological impairments and inflammation via enhancement of Nrf2 expression in rats. Pathophysiology. 2021;28(1):98–115. doi:10.3390/pathophysiology28010009
[64] Ni LL, Che YH, Sun HM, et al. The therapeutic effect of wasp venom (Vespa magnifica, Smith) and its effective part on rheumatoid arthritis fibroblast-like synoviocytes through modulating inflammation, redox homeostasis and ferroptosis. J Ethnopharmacol. 2023;317:116700. doi:10.1016/j.jep.2023.116700
[65] Zhang Y, Zhou M, Wang D, et al. Arsenic exposure and oxidative damage to lipid, DNA, and protein among general Chinese adults: a repeated-measures cross-sectional and longitudinal study. J Environ Sci. 2025;147:382–391. doi:10.1016/j.jes.2023.12.002
[66] Yang J, Wu J, Xie X, et al. Perilipin-2 mediates ferroptosis in oligodendrocyte progenitor cells and myelin injury after ischemic stroke. Neural Regen Res. 2025;20(7):2015–2028. doi:10.4103/NRR.NRR-D-23-01540
[67] Doll S, Proneth B, Tyurina YY, et al. ACSL4 dictates ferroptosis sensitivity by shaping cellular lipid composition. Nat Chem Biol. 2017;13(1):91–98. doi:10.1038/nchembio.2239
[68] Dodson M, Castro-Portuguez R, Zhang DD. NRF2 plays a critical role in mitigating lipid peroxidation and ferroptosis. Redox Biol. 2019;23:101107. doi:10.1016/j.redox.2019.101107
[69] Šribar J, Kovačič L, Oberčkal J, et al. The neurotoxic secreted phospholipase A(2) from the Vipera a. ammodytes venom targets cytochrome c oxidase in neuronal mitochondria. Sci Rep. 2019;9(1):283. doi:10.1038/s41598-018-36461-6
[70] Ravanan P, Srikumar IF, Talwar P. Autophagy: the spotlight for cellular stress responses. Life Sci. 2017;188:53–67. doi:10.1016/j.lfs.2017.08.029
[71] Costal-Oliveira F, Stransky S, Guerra-Duarte C, et al. L-amino acid oxidase from Bothrops atrox snake venom triggers autophagy, apoptosis and necrosis in normal human keratinocytes. Sci Rep. 2019;9(1):781. doi:10.1038/s41598-018-37435-4
[72] Ashrafi G, Schwarz TL. The pathways of mitophagy for quality control and clearance of mitochondria. Cell Death Differ. 2013;20(1):31–42. doi:10.1038/cdd.2012.81
[73] Dombi E, Mortiboys H, Poulton J. Modulating mitophagy in mitochondrial disease. Curr Med Chem. 2019;25(40):5597–5612. doi:10.2174/0929867324666170616101741
[74] Pickles S, Vigié P, Youle RJ. Mitophagy and quality control mechanisms in mitochondrial maintenance. Curr Biol. 2018;28(4):R170–R185. doi:10.1016/j.cub.2018.01.004
[75] Tang X, Wei T, Guan M, et al. Phospholipase A(2) induces acute kidney injury by complement mediated mitochondrial apoptosis via TNF-α/NF-κB signaling pathway. Food Chem Toxicol. 2023;172:113591. doi:10.1016/j.fct.2022.113591
[76] Fan X, Song Y, Liu Y, et al. Effect of cytochrome c release on the mitochondrial-dependent apoptosis and quality deterioration of black rockfish (Sebastes schlegelii) postmortem storage. Food Chem. 2024;458:140283. doi:10.1016/j.foodchem.2024.140283